Tennessee Valley Authority Kingston Fossil Plant Harriman, Roane County, Tennessee	**Perimeter Containment** **North Dredge Cell (Dike C) Segment 1** **Sta. A161+50 to A179+50**
Document Control Number RDP-0113-E *Calculation Package* FPGKIFFESCDX00030020100006	

Exhibit 11
Liquefaction Analysis

Purpose:

- Assess the potential for liquefaction to occur within the saturated ash and natural soil deposits during a design seismic event.

Methods:

- Empirical methods based on in situ SPT and CPT penetration resistance.
- Follow the NCEER procedure as defined by Youd et al (2001), but with updated factors from more recent research and publications.
- The calculations were completed using spreadsheets.

Results:

- Evaluated performance during the two design earthquake scenarios:
  - 2,475-year, $\mathbf{M_w}$=6.0 local event
  - 2,475-year, $\mathbf{M_w}$=7.6 New Madrid event

- Extensive liquefaction is predicted within the saturated deposits of hydraulically placed ash and natural alluvial silt/sand

Calculation Performed by: Stantec Consulting Services, Inc.	
Prepared by: YW 10-Nov-10	*Reviewed by:* JSD 11-Nov-10
Revisions:	

Liquefaction Triggering Analyses

The purpose of the liquefaction triggering analyses is to assess the potential for liquefaction to occur within the saturated, hydraulically placed ash and natural alluvial soil deposits during design earthquake events. Residual strengths will be assigned to the liquefied materials in slope stability analyses under post-earthquake conditions.

1.1. Magnitude-Distance Correlation

Compared to smaller events, larger magnitude earthquakes are capable of causing damage at greater distances. Ambraseys (1988) compiled magnitude, epicentral distance, and whether or not liquefaction was observed at various locations in past earthquakes. The data (Figure 1.1) illustrate an approximate threshold for combinations of magnitude and epicentral distance that are necessary to cause liquefaction. However, the simple empirical relationship represented in Figure 1.1 does not account for attenuation characteristics that differ in various geologic settings and site-specific soil conditions. For example, seismic events in the central U.S. are known to generate strong ground motions over larger distances than west-coast earthquakes. Hence, a boundary line drawn on Figure 1.1 for central U.S. events would be expected to fall to the right of a boundary line drawn for western U.S. events. Ambraseys' threshold line is sometimes used, by organizations such as the U.S. Bureau of Reclamation, as a screening tool to identify sites where liquefaction needs to be assessed. Figure 1.1 can also be used to check the reasonableness of results from more detailed analyses.

The design earthquake events for the Kingston closure option, estimated in the site-specific study performed by AMEC (Exhibit 7), are plotted on Figure 1.1. The two candidate design events fall below, but relatively close to the historical threshold. Considering the different attenuation effects noted above, the appropriate threshold line could be farther to the right and encompass one or both events. This simple empirical evidence suggests that liquefaction might occur at Kingston during an M_w = 6.0 event in the local vicinity (R = 36 km) and/or during an M_w = 7.6 event from the New Madrid Seismic Zone (R = 435 km). Clearly, more detailed analysis of the liquefaction potential is warranted.

1.2. Empirical Evaluation of Liquefaction Potential

Seed and Idriss (1971) proposed a simplified procedure for evaluating liquefaction potential based on soil type, relative density or void ratio, initial confining stress and intensity of ground shaking. This methodology has undergone continued development and refinement since its initial inception. The methodology was evaluated in detail and summarized by a workshop of experts organized by the National Center for Earthquake Engineering Research (NCEER) (Youd and Idriss 1997). This updated liquefaction assessment method, as summarized by Youd et al. (2001), is often referred to as the "NCEER Method" and is summarized in Sections 1.4 through1.7. For certain parameters, the results of more recent research have provided new correlations or assumptions that have been utilized in this study. These differences from the Youd et al. (2001) methodology are identified below, where applicable.

The NCEER method compares the liquefaction resistance of a soil, expressed in terms of a Cyclic Resistance Ratio (*CRR*), to the Cyclic Stress Ratio (*CSR*) induced by the design earthquake. Both the *CRR* and *CSR* represent a shear stress normalized with respect to the vertical effective stress in the soil. The factor of safety with respect to soil liquefaction is then computed as the ratio of *CRR* to *CSR* (Section 1.7). Criteria for fine-grained soils (Section1.3) can be used to screen for potentially liquefiable clays and silts.

The cyclic resistance ratio (*CRR*) can be determined through cyclic laboratory testing, but is more commonly estimated using empirical correlations developed for various in situ tests. In this assessment of the closure plan, the *CRR* was estimated using Standard Penetration Test (SPT) and Cone Penetration Test (CPT) data, as discussed in the remainder of this report.

The cyclic stress ratio (*CSR*) induced by the earthquake is the average shear stress ratio, assumed to be 65% of the maximum induced shear stress ratio. In this study of the closure plan, the *CSR* was computed in the one-dimensional ground response analysis carried out using the computer program *ProShake*. Details of the *ProShake* analysis along with the obtained results are presented in Exhibit 10. The simplified equation for estimating *CSR* (Seed and Idriss 1971), based on an average stress reduction factor, was not used in this study.

1.3. Liquefaction Susceptibility of Fine-Grained Soils

While liquefaction is usually associated with sand deposits, fine-grained soils have been observed to liquefy in large earthquakes. Seed and Idriss (1982) suggested that clayey soils could be evaluated for liquefaction susceptibility based on clay content, liquid limits, and natural water content, using criteria developed from field observations in China. However, recent research by Seed et al. (2003) refers to several case histories where liquefaction was documented in soils that contained enough plastic fines to be classified as non-liquefiable under the older criteria.

Seed et al. (2003) proposed new criteria (Figure 1.2) for identifying potentially liquefiable soils with significant fines content. The fines content, liquid limit, plasticity index, and natural water content are taken into consideration. Soils that fall in Zone A and meet the water content requirement should be considered potentially liquefiable and can be evaluated using the NCEER method. Soils that fall in Zone B and meet the water content requirement may be potentially liquefiable, but are not typically suitable for penetration testing associated with the NCEER method. Soils that fall in Zone C (i.e., anywhere else on the chart) are not subject to liquefaction, but could be sensitive and experience strength loss with remolding or large monotonic shear displacements. Clayey soils encountered at the Dredge Cell site with Atterberg limits test performed are shown in Figure 1.3.

1.4. Liquefaction Resistance from SPT Data

1.4.1. Normalized, Corrected SPT Blowcount $(N_1)_{60}$

The liquefaction assessment was accomplished using “corrected, clean-sand equivalent” SPT blowcounts, $(N_1)_{60\text{-}CS}$, wherein the penetration resistance measured in the field was corrected, adjusted, and/or normalized to account for the effects of overburden pressure, hammer energy, borehole diameter, length of drill rods, nonstandard samplers, and fines

content. The NCEER method of liquefaction assessment (Youd et al. 2001) includes recommended relationships, summarized in this section, for computing $(N_1)_{60\text{-}CS}$ from measured N_{SPT} values.

First, the corrected, normalized blowcount, $(N_1)_{60}$, is computed from:

$$(N_1)_{60} = N_{SPT} C_N C_E C_B C_R C_S \qquad \textbf{Eqn. 1.1}$$

The correction parameters (C_N, C_E, C_B, C_R, and C_S) are defined as follows.

C_N is used to normalize N_{SPT} to an equivalent value (N_1) that would be measured under one atmosphere of overburden pressure. Trends in the available data for C_N are shown in Figure 1.4. Youd et al. (2001) list two equations (Figure 1.4) that can be used to approximate C_N; Eqn. 1.2 was used in this project because it is reported to provide a better fit to the available data for overburden pressures exceeding 4,000 psf.

$$0.5 \le \left(C_N = \frac{2.2}{1.2 + \left(\sigma'_{vo} / P_a\right)} \right) \le 1.7 \qquad \textbf{Eqn. 1.2}$$

Here, σ'_{vo} = vertical effective stress at depth of N_{SPT} and P_a = 1 atmosphere pressure (101 kPa ≈ 2,116 psf). The value of C_N is limited to 1.7 to avoid excessively large adjustments at very low pressures (σ'_{vo} less than about 200 psf). For pressures exceeding about 6,770 psf, where the correction is poorly defined, the value of C_N was set to a limit of 0.5.

C_E corrects N_{SPT} for differences in SPT hammer energy, using as a standard reference a hammer that delivers 60% of the maximum theoretical energy (140-lbs x 30-inch drop = 350 ft-lbs per blow). Defining the energy ratio (*ER*) as the actual energy delivered by the SPT hammer over the maximum theoretical energy, the value of C_E is then:

$$C_E = \frac{ER}{60\%} \qquad \textbf{Eqn. 1.3}$$

When the hammer energy is not measured, the typical ranges given in Table 1.1Table can be used. The SPT tests completed at Kingston Dredge Cell included energy measurements for selected intervals for each drill rig used (GRL Engineers, Inc. 2009). A short section of drill rod at the top of the drill string was instrumented with accelerometers and strain gages, which permitted electronic determination of the delivered energy using the "*Fv*" (force-velocity) method (Butler et al. 1998). Energy measurements were collected and processed using the SPT Analyzer® and associated software, both from Pile Dynamics, Inc. (Cleveland, Ohio). The energy transmission ratio (*ETR*) reported by the SPT Analyzer® for each blow was averaged over the depth of penetration (18 in.) in each SPT test. This average *ETR* was used as the hammer energy ratio (*ER*) in correcting the measured blowcounts according to Eqn. 1.3.

A minimum of five SPT intervals were measured for hammers on six different drill rigs. Stantec reviewed the data and assigned average *ER* (and thus C_E) values to each hammer (Table 1.2) for use in N_{SPT} corrections and subsequent liquefaction calculations.

Average values were assigned because there were no significant trends with depth and the standard deviation was small for *ER* readings for each particular hammer.

C_B corrects for disturbance in large boreholes, based on the borehole diameter (internal diameter of casing or hollow stem auger). Recommended values are given in Table 1.3a. To apply this correction without making sharp jumps in C_B for small differences in diameter, the values in Table 1.3a were linearly interpolated for diameters in the range of 4.5 to 8 inches (Table 1.3b).

C_R corrects for energy losses in short drilling rods, due to reflections of energy from the bottom of the drill stem. Values recommended by Youd et al. (2001) are given in Table 1.4. In applying this correction, the length of drill rod was assumed to equal the depth to the sampling location, plus 5 ft to account for the typical length of drill rod sticking up above the ground surface. For deeper sample locations (rod lengths exceeding 30 m), no correction was applied (C_R = 1.0). However, for SPT borings performed by drill rigs and hammers which had values of C_E derived from site-specific energy measurements, no rod length correction was applied (C_R = 1.0), based on the information presented below.

Values of the rod length correction factor (C_R, Table 1.4) were originally recommended by Skempton (1986), but are based on the work of Schmertmann and Palacios (1979). Due to limitations in the instrumentation available at the time of their work, Schmertmann and Palacios were unable to accurately measure accelerations in the drill rod after each impact. They measured hammer energy using the "F^2" method and proposed the rod-length correction based on theoretical considerations of wave propagation. The "*Fv*" method of measuring delivered hammer energy, used in the 2009 investigation of the Kingston Dredge Cell area, provides a more reliable measure of hammer energy (Butler et al. 1998) and obviates the need to make corrections for short rods (personal communications, Frank Rausche, April 15, 2005, and Ray B. Seed, April 20, 2005). Additional insights into the application of C_R are provided by Youd et al. (2001):

> *Although application of rod-length correction factors … will give more precise $(N_1)_{60}$ values, these corrections may be neglected for liquefaction resistance calculations for rod lengths between 3 and 10 m because rod-length corrections were not applied to SPT test data from these depths in compiling the original liquefaction case history databases. Thus rod-length corrections are implicitly incorporated into the empirical SPT procedure*.

Daniel et al. (2005) point out the need for more research on this question. For the N_{SPT} values measured at Kingston, the C_R correction was not applied to the 2009 data where hammer energy was measured (or implied, based on use of the same drill rig and hammer) using the "*Fv*" method, but was applied to all other data where hammer energy was assumed.

C_S corrects for standard split-spoon samplers that are used without the liners. Recommended values are shown in Table 1.5. Although NCEER guidance for liquefaction analysis recommends the use of liners, the liners are commonly omitted, thus reducing the interior friction as the SPT is performed. When liners are not used, the correction ranges from 10 to 30 percent, and increases linearly as the blowcount increases. At Kingston, all SPT samples were collected using standard samplers without liners, so appropriate correction factors have been applied in the analysis.

1.4.2. Clean-Sand Equivalent SPT Blowcount $(N_1)_{60\text{-CS}}$

The fines content (percent passing the No. 200 sieve) can have a significant impact on liquefaction resistance. All else being equal, liquefaction susceptibility decreases as the fines content and/or plasticity of a soil increases.

The NCEER method of assessing liquefaction potential (Youd et al. 2001) utilizes an adjustment in $(N_1)_{60}$ to account for variations in cyclic strength and penetration resistance due to the fines content of coarse-grained soils. The "clean-sand equivalent blowcount", $(N_1)_{60\text{-}CS}$, is computed using Eqn. 1.4 and the parameters in Table 1.6.

$$(N_1)_{60-CS} = \alpha + \beta(N_1)_{60} \qquad \textbf{Eqn. 1.4}$$

The adjustment from $(N_1)_{60}$ to $(N_1)_{60\text{-}CS}$ was developed using data on liquefaction resistance. Hence, $(N_1)_{60\text{-}CS}$ reflects both the increase in liquefaction resistance and decrease in penetration resistance due to a fines content greater than 5% (Youd et al. 2001).

Where the gradation of an individual SPT sample is not measured in the laboratory, the calculation of $(N_1)_{60\text{-}CS}$ must rely on an estimated fines content. The fines content (*FC*) associated with a specific N_{SPT} value was thus determined, in decreasing order of priority, as:

- Where SPT samples were subjected to particle size analysis, *FC* was taken from the laboratory value recorded on the boring log.
- When the gradation was not measured on a given sample, *FC* was estimated by roughly interpolating between measured values, from samples in the same soil horizon and soil boring, immediately above and below the SPT location.
- When no gradation data was available for a given soil horizon, the fines content was assigned based on the USCS classification, assuming the minimum fines content for that soil classification. This yields a conservative correction (smallest corrected $(N_1)_{60\text{-}CS}$) for determining liquefaction resistance.

In consideration of the unique characteristics of the materials at the site and to avoid inappropriately inflating the liquefaction resistance, it was agreed upon by Stantec, AECOM, URS and TVA that the above fines content corrections will not be applied to the fly ash or where SPT blowcounts of "weight of hammer" or "weight of rods" are recorded. Since labeling a soil as fly ash can be subjective and the fly ash typically contains high fines contents, in the analysis silts with fines content greater than or equal to 50 percent was considered as fly ash. Therefore, the above fines content corrections were only applicable to the soils with fines content less than 50 percent and SPT blowcounts greater than zero.

1.4.3. $CRR_{7.5}$ from SPT Blowcount

The cyclic resistance ratio (*CRR*) of the soil, or the shear stress required to cause liquefaction under field conditions, was determined from the corrected SPT blowcounts,

$(N_1)_{60\text{-}CS}$, and the NCEER field performance correlation. The cyclic resistance ratio for a magnitude (moment magnitude) M_w = 7.5 earthquake ($CRR_{7.5}$) is estimated from the $(N_1)_{60\text{-}CS}$ using the "SPT Clean Sand Base Curve" in Figure 1.5. For values of $(N_1)_{60\text{-}CS}$ less than 30, the following equation for the base curve was developed by A. F. Rauch (Youd et al. 2001):

$$CRR_{7.5} = \frac{1}{34-(N_1)_{60-CS}} + \frac{(N_1)_{60-CS}}{135} + \frac{50}{\left[10\cdot(N_1)_{60-CS}+45\right]^2} - \frac{1}{200} \qquad \textbf{Eqn. 1.5}$$

For values of $(N_1)_{60\text{-}CS}$ greater than or equal to 30, clean granular soils are too dense to liquefy and are classified as non-liquefiable.

Table 1.1. Typical correction factors for SPT hammer energy (Youd et al. 2001).

Hammer Type	ER	C_E
Safety Hammer	42 to 72%	0.7 to 1.2
Automatic-trip (Donut) Hammer	48 to 78%	0.8 to 1.3

Table 1.2. Kingston correction factors for SPT hammer energy (data from GRL Engineers, Inc. 2009).

Drill Rig and Hammer Type	Avg. ER (%)	ER Std. Dev. (%)	C_E
CME 850, Automatic Hammer	79	2	1.32
Diedrich D-25, Safety Hammer	78	2	1.30
Diedrich D-50, Automatic Hammer	56	2	0.93
Diedrich D-120, Automatic Hammer	78	4	1.30
Mobile B-57 (SN #DR-35), Automatic Hammer	93	3	1.55
Mobile B-57 (SN #91034)	88	3	1.47

Table 1.3. Correction factors for borehole diameter.

Inner Diameter (ID) of Casing or Auger (inches)	C_B
(a) Typical values (Youd et al, 2001)	
2.5 to 4.5	1.00
6	1.05
8	1.15
(b) Interpolated values	
ID ≤ 4.5	C_B = 1.00
4.5 < ID ≤ 6	C_B = (ID/30) + 0.85
6 < ID ≤ 8	C_B = (ID/20) + 0.75
8 < ID	C_B = 1.15

Table 1.4. Correction factors for energy losses in the drill rods (Youd et al. 2001).

Length of Drill Rod (m)	C_R
< 3 m	0.75
3 to 4	0.8
4 to 6	0.85
6 to 10	0.95
10 to 30	1.0
Note: No rod length correction factor applied (i.e., C_R = 1.0) when hammer energy is measured using the "Fv" method (see Section 1.4.1).	

Table 1.5. Correction factors for SPT sampler liners (Youd et al. 2001).

Sampler	C_S
Standard split-spoon sampler with liners	1.0
Standard split-spoon sampler without liners	$1.1 \leq 1+(N_1)_{60}/100 \leq 1.3$

Table 1.6. Parameters for computing $(N_1)_{60\text{-}CS}$ (Youd et al. 2001).

FC *	A	β
FC ≤ 5%	α = 0	β = 1.0
5% < FC < 35%	$ln(\alpha) = 1.76-(190/FC^2)$	$\beta = 0.99+(FC^{1.5}/1000)$
FC ≥ 35%	α = 5.0	β = 1.2

* FC = fines content, percent by weight finer than 0.075 mm

1.5. Liquefaction Resistance from CPT Data

1.5.1. Normalized, Corrected Cone Penetration Resistance (q_{c1N})

The measured resistance to penetration of the conical CPT tip (q_c), in units of stress, is recorded as the cone penetrometer probe is advanced into the soil. Due to details of the probe design, pore water pressures acting behind the cone tip affect the measurement of tip resistance. A corrected cone tip resistance (q_t) is computed as:

$$q_t = q_c + (1 - A) \cdot u_2 \qquad \textbf{Eqn. 1.6}$$

where A is the net area ratio and u_2 is the pore water pressure measured just behind the cone tip.

The CPT tip resistance data from Kingston, collected by AECOM, was reported in terms of q_t, and the correction from q_c was not provided. The differences between q_c and q_t are usually small in granular soils, while the effect of the correction in Eqn. 1.6 is more significant in soft, saturated soils where q_c is small and u_2 is large.

The tip resistance is corrected for the effects of overburden pressure and normalized to a dimensionless value using (Robertson and Wride 1998; Youd et al. 2001):

$$q_{c1N} = C_Q \left(\frac{q_t}{P_a} \right) \qquad \textbf{Eqn. 1.7}$$

where P_a is one atmosphere of pressure in the units of q_t. C_Q is computed as:

$$C_Q = \left(\frac{P_a}{\sigma'_{vo}} \right)^n \leq 1.7 \qquad \textbf{Eqn. 1.8}$$

where σ'_{vo} is the vertical effective stress at the location of the measurement q_t and P_a is one atmosphere of pressure in the units of σ'_{vo}. The exponent n varies from 0.5 to 1.0, depending on soil type, and can be selected iteratively based on the value of I_c as described below. A limit of 1.7 is placed on C_Q to avoid excessive corrections at shallow depths.

Using CPT data, soil behavior can be classified using the chart in Figure 1.6 (Robertson 1990). The classification is based on a normalized cone resistance (Q):

$$Q = \left(\frac{q_t - \sigma_{vo}}{P_a} \right) \left(\frac{P_a}{\sigma'_{vo}} \right)^n \qquad \textbf{Eqn. 1.9}$$

where the variables are as defined previously. The classification chart also uses the normalized friction ratio (F):

$$F = \left(\frac{f_s}{q_t - \sigma_{vo}} \right) \times 100\% \qquad \textbf{Eqn. 1.10}$$

where f_s is the measured sleeve resistance (units of stress). The boundaries between soil types 2 to 7 in Figure 1.6 can be approximated using concentric circles having radii equal to the soil behavior type index (I_c):

$$I_c = \left[(3.47 - \log Q)^2 + (1.22 + \log F)^2 \right]^{0.5} \qquad \textbf{Eqn. 1.11}$$

The value of the exponent (n) in Eqn. 1.8 and Eqn. 1.9 depends on the soil type, necessitating a three-step iterative solution scheme (Robertson and Wride 1998; Youd et al. 2001):

- *Step 1*: Assume n = 1.0 (characteristic of clays) and compute I_c from Eqn. 1.9 through Eqn. 1.11. If I_c > 2.6, the soil is classified as clayey and n = 1.0 is used. Such soils typically do not liquefy (Section 1.3).

- *Step 2*: If I_c < 2.6 in Step 1, assume n = 0.5 (characteristic of granular soils) and re-compute I_c from Eqn. 1.9 through Eqn. 1.11. If I_c < 2.6, then use n = 0.5 to further evaluate liquefaction resistance.

- *Step 3*: If I_c > 2.6 in Step 2, the soil is probably very silty and possibly plastic. In this case, evaluate the liquefaction resistance using an intermediate value of n = 0.7.

In addition, soils with I_c > 2.6 and F < 1% will plot in region 1 of Figure 1.6; such soils may be very sensitive and should be appropriately evaluated for liquefaction resistance.

1.5.2. Clean-Sand Equivalent Cone Penetration Resistance $(q_{c1N})_{cs}$

The fines content (percent passing the No. 200 sieve) of a soil can have a significant impact on liquefaction resistance. For silty sands, the NCEER methodology for liquefaction assessment (Youd et al. 2001) includes the calculation of a "clean-sand equivalent penetration resistance", $(q_{c1N})_{cs}$:

$$(q_{c1N})_{CS} = K_c \cdot q_{c1N} \qquad \textbf{Eqn. 1.12}$$

where q_{c1N} is the normalized, corrected cone tip resistance (Eqn. 1.7) and K_c is a correction factor for grain characteristics.

The variation of K_c with soil behavior type index (I_c, Eqn. 1.11) is plotted in Figure 1.7. In equation form, K_c is computed as (Robertson and Wride 1998; Youd et al. 2001):

$$\begin{aligned} &For \quad I_c \le 1.64: \quad K_c = 1.0 \\ &For \quad I_c > 1.64: \quad K_c = -0.403 I_c^4 + 5.58 I_c^3 - 21.63 I_c^2 + 33.75 I_c - 17.88 \qquad \textbf{Eqn. 1.13} \\ &For \quad 1.64 < I_c < 2.36 \; and \; F < 0.5\%: \quad K_c = 1.0 \end{aligned}$$

Note that the relationship for K_c is shown as a dashed line in Figure 1.7 for I_c > 2.6. Soils in this regime (Figure 1.6) would classify as clayey silt, silty clay, or clay, with a fines content greater than about 35%. In most cases, such soils are unlikely to liquefy due to their clay content. However, due to the unique nature of fly ash (essentially a potentially liquefiable, non-plastic silt), the classification as a fine-grained soil and fines content greater than 35% is not sufficient to rule out liquefaction.

As discussed in Section 1.4.2, it was agreed upon that the grain characteristic corrections will not be applied to the fly ash deposit. In the analysis, no corrections were performed for soils with I_c greater than 2.6 (set K_c = 1 for these soils). Although some fly ash mixtures with I_c ≤ 2.6 still ended up being corrected for fines content, it was anticipated that very silty or clayey deposits (including majority of the fly ash) were not subjected to fines correction.

1.5.3. $CRR_{7.5}$ from CPT Tip Resistance

The cyclic resistance ratio (*CRR*) of the soil, or the shear stress required to cause liquefaction under field conditions, was determined from the measured CPT tip resistance and the NCEER field performance correlation (Robertson and Wride 1998; Youd et al. 2001).

Field measurements of CPT tip stress were first normalized and adjusted to account for the effects of overburden pressure and fines content, as described in Section 1.5.1 and

Section 1.5.2, respectively. The cyclic resistance ratio for a magnitude M_w = 7.5 earthquake ($CRR_{7.5}$) was estimated using the correlation suggested by Robertson and Wride (1998; Youd et al. 2001) and shown in Figure 1.8. The following equations represent the CPT-based clean sand base curve, and can be used to compute $CRR_{7.5}$:

$$For \quad (q_{c1N})_{CS} < 50: \quad CRR_{7.5} = 0.833\left[\frac{(q_{c1N})_{CS}}{1{,}000}\right] + 0.05$$

$$For \quad 50 \le (q_{c1N})_{CS} < 160: \quad CRR_{7.5} = 93\left[\frac{(q_{c1N})_{CS}}{1{,}000}\right]^3 + 0.08$$

Eqn. 1.14

where $(q_{c1N})_{cs}$ is the clean-sand equivalent penetration resistance normalized to one atmosphere of overburden pressure.

1.6. Adjusted Cyclic Resistance Ratio

To account for other earthquake magnitudes, $CRR_{7.5}$ (estimated from either SPT or CPT data) is modified using a magnitude scaling factor. Adjustments are also made to account for high overburden pressures and static driving shear stresses. The *CRR* of the soil is then computed as:

$$CRR = CRR_{7.5} \cdot MSF \cdot K_\sigma \cdot K_\alpha$$

Eqn. 1.15

The correction factors *MSF*, K_σ and K_α are discussed below.

Because the simplified procedure was originally developed using a database of case histories from earthquakes near magnitude M_w = 7.5, a magnitude scaling factor (*MSF*, Section 1.6.1) must be applied to account for the greater number of significant stress cycles experienced in larger magnitude earthquakes. In addition, the simplified procedure was developed using data from sites with a level to gently sloping surface and soil depths less than about 45 feet. Using laboratory test data, Seed (1983) proposed two corrections to adjust the *CRR* for high static overburden stress and static shear stress imposed by a sloping ground surface. The K_σ correction factor (Section 1.6.2) thus extends the simplified procedure to higher overburden stresses and the K_α correction factor (Section 1.6.3) permits the consideration of more steeply sloping ground conditions. These factors can be significant when considering the liquefaction resistance of soils beneath large embankments.

1.6.1. Magnitude Scaling Factor

There have been many different suggestions for the relationship between magnitude scaling factor (*MSF*) and earthquake magnitude (Figure 1.9). With recently developed new correlations for K_σ and K_α (Section 1.6.2 and 1.6.3), Idriss and Boulanger (2008) suggested using Eqn. 1.16 for *MSF*, which was actually the *MSF* published by Idriss (1999).

$$MSF = 6.9\exp(-0.25M_w) - 0.058 \le 1.8$$

Eqn. 1.16

According to Eqn. 1.16, the New Madrid earthquake (M_w = 7.6) results in an *MSF* = 0.97 and the local earthquake (M_w = 6.0) results in an *MSF* = 1.48.

1.6.2. Correction for Overburden Stresses

Laboratory data show a nonlinear increase in liquefaction resistance with an increase in effective confining pressure. Hynes and Olsen (1999) developed a set of curves relating K_σ to vertical effective stress for soils of different relative densities. The NCEER workshop endorsed these curves for use in engineering practice for clean sand, silty sands and gravels (Youd et al. 2001).

More recent work published by Boulanger (2003a) and Idriss and Boulanger (2008) has investigated this issue further and has resulted in new curves (Figure 1.10) for K_σ. The more recent relationships shown in Idriss and Boulanger (2008) have been used herein, although the upper bound of K_σ has been set to 1.0, instead of their suggested 1.1. A cap of 1.0 is consistent with the results of the NCEER workshop, and avoids additional increase of liquefaction resistance at low confining pressures due to generation of negative pore pressures (which are typically ignored) in dilative soils. The overburden correction factors in Figure 1.10 can be expressed:

$$K_\sigma = 1 - C_\sigma \cdot \ln\left(\frac{\sigma'_{vo}}{P_a}\right) \leq 1.0 \qquad \textbf{Eqn. 1.17}$$

where P_a is one atmospheric pressure in the units of the vertical effective stress, σ'_{vo}. C_σ is a coefficient expressed in terms of relative density:

$$C_\sigma = \frac{1}{18.9 - 17.3 \cdot D_R} \leq 0.3 \qquad \textbf{Eqn. 1.18}$$

Consistent with relationships shown in Idriss and Boulanger (2008), relative densities were estimated using correlations to SPT blowcounts and CPT tip resistance, as shown below:

$$D_R = \sqrt{\frac{(N_1)_{60}}{C_d}} \qquad \textbf{Eqn. 1.19}$$

where C_d is a parameter that is a function of the type of sand. For this study, C_d = 46 was used, which is consistent with the value used by Idriss and Boulanger (2008) to check liquefaction triggering correlations. This value of C_d results in an upper bound $(N_1)_{60}$ value of 46 in order to remain in a valid range of relative density. The correlation for CPT tip resistance is:

$$D_R = 0.465 \cdot \left(\frac{q_{c1N}}{C_{dq}}\right)^{0.264} - 1.063 \qquad \textbf{Eqn. 1.20}$$

where C_{dq} is a parameter that is a function of the type of sand. For this study, C_{dq} = 0.9 was used, which is consistent with the value used by Idriss and Boulanger (2008) to check liquefaction triggering correlations. This value of C_{dq} results in a lower bound q_{c1N} value of 21 and an upper bound q_{c1N} value of 254 in order to remain in a valid range of relative density.

The above correlations are based on laboratory tests and/or case histories for sands, and the suitability of such correlations is uncertain for the ash materials at Kingston. However, lacking more suitable correlations, it seems reasonable (for derivation of this property) to assume that the cohesionless ash materials behave similar to sand.

1.6.3. Correction for Static Shear Stresses

A sloping ground surface creates driving shear stresses in the soil mass under static conditions. The static driving shear stresses can be represented by alpha (α), which is the ratio of the static driving shear stress (τ_{hv}) acting on a horizontal plane to the vertical effective stress (σ'_{vo}):

$$\alpha = \frac{\tau_{hv}}{\sigma'_{vo}} \qquad \textbf{Eqn. 1.21}$$

Static shear stress increases the cyclic resistance of a dense soil under low confining pressure, because higher induced shear stresses are required to cause stress reversal. However, loose soils and some soils under high confining pressures have lower cyclic resistance due to strain softening behavior. The K_α parameter, which is used to modify the *CRR* for this effect, can vary widely depending upon the value of alpha and the relative density of the soil (see Figure 1.11). Because K_α is poorly defined, K_α is often assumed to be one (no adjustment in *CRR*) in liquefaction assessments.

However, recent research presented by Boulanger (2003b) and Idriss and Boulanger (2008) has provided a more substantial basis for applying the K_α parameter to modify the *CRR*. Given the significance of the issue for Kingston and the fact that an assumption of K_α = 1 could be unconservative for a loose (contractive) soil beneath a slope, it is reasonable to adopt these new procedures in liquefaction triggering analysis.

Alpha (α) can be estimated by performing a stress analysis of a typical cross section using *SIGMA/W* (GEO-SLOPE International, Calgary, Canada), which is a stress and deformation analysis software product. A Poisson's ratio v = 0.33 was assigned to all soils. The value of the Poisson's ratio was determined from Eqn. 1.22, assuming the at-rest lateral earth pressure coefficient K_o = 0.5. Contour maps of τ_{hv} and σ'_{vo} were generated for the typical cross section in *SIGMA/W* (Figures 1.12 and 1.13). Four profiles (Figure 1.14), approximately representing relative SPT and CPT locations with respect to the proposed perimeter berm, were defined. Borings associated with each profile are summarized in Table 1.7. Values of τ_{hv} and σ'_{vo} were extracted along each profile and α versus depth was then calculated. Finally, a fourth-order polynomial curve was fit through the data points to define the α value at any depth in a soil profile. The four fit curves along with their equations are presented in Figures 1.15 through 1.18. These equations were then utilized in the liquefaction triggering analysis at each SPT and CPT location.

$$\nu = \frac{K_o}{1 + K_o} \qquad \textbf{Eqn. 1.22}$$

Table 1.7. SPT/CPT locations associated with profiles used in computing α

Profile	Ground Surface Elevation	CPT/SPT Holes Represented
1	El. 790	09-301 through 09-304 09-500 through 09-503 09-600 through 09-605
2	El. 790	09-100 through 09-110
3	El. 765	09-200; 09-211 09-400 through 09-413
4	El. 750	09-201 through 09-210

Idriss and Boulanger (2008) present K_α as a function of α and a relative state parameter index (ξ_R), which is the difference between the actual relative density (D_R) and an empirical critical state relative density ($D_{R,CS}$). The critical state relative density is a function of grain type (as it relates to particle crushing) and mean effective stress. Several equations from Idriss and Boulanger (2008) are presented below that are used to arrive at K_α.

$$\xi_R = D_{R,CS} - D_R$$

$$D_{R,CS} = \frac{1}{Q - \ln\left[\frac{100 \cdot (1 + 2 \cdot K_o) \cdot \sigma'_{vo}}{3 \cdot P_a}\right]} \qquad \textbf{Eqn. 1.23}$$

where Q is a function of grain type (assumed to be 10, corresponding to quartz sand), at-rest lateral earth pressure coefficient K_o is assumed to be 0.5, and D_R is estimated from SPT data (Eqn. 1.19) or CPT data (Eqn. 1.20).

After α and ξ_R have been calculated, K_α can be estimated as follows:

$$K_\alpha = a + b \cdot \left(\frac{-\xi_R}{c}\right)$$

$$a = 1{,}267 + 636 \cdot \alpha^2 - 634 \cdot \exp(\alpha) - 632 \cdot \exp(-\alpha) \qquad \textbf{Eqn. 1.24}$$

$$b = \exp\left[-1.11 + 12.3 \cdot \alpha^2 + 1.31 \cdot \ln(\alpha + 0.0001)\right]$$

$$c = 0.138 + 0.126 \cdot \alpha + 2.52 \cdot \alpha^3$$

Eqn. 1.24 is based on data shown in Figure 1.11, and thus should be constrained within the following limits: $\alpha \leq 0.35$ and $-0.6 \leq \xi_R \leq 0.1$.

The above K_α correlations are based on laboratory and/or case histories for sands, and the suitability of such correlations is uncertain for the ash materials at Kingston. Also, the data shown in Figure 1.11 are based primarily on simple shear tests and a failure

criterion of 3% shear strain. Available laboratory test data indicate that some of the ash deposits at Kingston are sensitive, such that failure within the ash may occur at a much lower shear strain, thus adding to the uncertainty of the K_α parameter utilized herein. However, lacking more suitable correlations, it seems reasonable (for derivation of this property) to assume that the cohesionless ash materials behave similar to sand.

The absolute values of calculated α ranged from 0 to the upper constrained limit of 0.35. For loose materials at the Kingston site, small K_α values (about 0.12) were computed. This indicated that the *CRR* of these soils would be significantly reduced by the presence of static shear stresses, which confirmed that it was unconservative to assume $K_\alpha = 1$ in the liquefaction triggering analysis. The calculated upper bound K_α value was about 2.5, which was obtained from dense soils at relatively shallow depths.

1.7. Factor of Safety against Liquefaction

The factor of safety against liquefaction (FS_{liq}) is computed as the ratio of *CRR* to *CSR*:

$$FS_{liq} = \frac{CRR}{CSR} \qquad \textbf{Eqn. 1.25}$$

Values of FS_{liq} computed with Eqn. 1.25 can be used to judge how a soil will behave in a given earthquake scenario. Contemporary geotechnical practice usually follows the precedent set by Seed and Harder (1990), who made the following assumptions:

- Where $FS_{liq} \leq 1.1$, the soil is expected to liquefy. In a post-earthquake static stability analysis, residual strengths can be assumed in these areas.
- Where $1.1 < FS_{liq} \leq 1.4$, substantial soil softening may occur, possibly leading to progressive failures.
- Where $FS_{liq} > 1.4$, the soil does not liquefy. Minor pore pressures may be generated, but the soil will retain a large portion of the static strength.

1.8. Results from Liquefaction Triggering Analyses

Two design earthquake scenarios were considered for the liquefaction triggering analyses (Local Earthquake: $M_w = 6.0$ and New Madrid Earthquake: $M_w = 7.6$). The analyses were performed using data from 46 SPT borings and 50 CPT tests located around/within the Kingston Dredge Cell (All these borings were performed by AECOM. While more borings around the Main Ash Pond and along Dike C were drilled by AECOM and Stantec, those borings were not analyzed). Each individual SPT and CPT measurement was analyzed. The earthquake loading at each data point was predicted by interpolating the results coming out from representative, one-dimensional ground response analyses (*ProShake*). The liquefaction resistance was estimated using the methods presented in Section 1.2 through 1.6. All analyses were completed by implementing these methods in a spreadsheet application.

Liquefaction potential of the alluvial lean clay foundation soils was evaluated using the screening procedures outlined in Section 1.3. First, all available Atterberg limits data obtained from the alluvial foundation soils classified as CL-ML or CL (a total of 112 samples) were plotted on a USCS fine-grained soil classification chart (Figure 1.3a).

Based on liquid limit (*LL*) and plasticity index (*PI*) only, 72 samples fell in Zone A and 32 samples fell in Zone B (Figure 1.3b). While also applying the screening criteria for natural moisture content and fines content (fines contents were determined according to procedures presented in Section 1.4.2), 55 samples in Zone A and 7 samples in Zone B met all criteria (Figure 6.3c). Assuming the above limited data are representative throughout the entire site, the results of this screening analysis indicate that about one half (55 out of 112) of the lean clay soil is susceptible to significant loss of strength or liquefaction in earthquake events.

Graphic presentations of the calculated factors of safety against liquefaction are included in Figures 1.19 through 1.28. For each design earthquake scenario, plots are presented showing the predicted factors of safety versus elevation along the following profiles. AECOM boring layout is shown in Figure 1.29.

- AECOM 100-Series Borings: approximately parallel to the Dredge Cell north boundary, about 200 feet from the centerline of the proposed perimeter berm, towards the Dredge Cell

- AECOM 200-Series Borings: approximately parallel to the Dredge Cell north boundary, roughly at the outside toe of the proposed perimeter berm

- AECOM 300- and 500-Series Borings: inside the Dredge Cell, relatively far away from the proposed perimeter berm

- AECOM 400-Series Borings: approximately parallel to Swan Pond Road, roughly at the centerline of the proposed perimeter berm

- AECOM 600-Series Borings: approximately following Dike D

The results indicate that at many data points, the calculated FS_{liq} is less than 1.1 under both design earthquake scenarios (Local and New Madrid). Liquefaction in the hydraulically placed fly ash and the alluvial sandy silt to silty sand soils are anticipated. Therefore, mitigation measures need to be carried out in developing closure plans for the Dredge Cell.

1.9. Assessment of Liquefaction

The liquefaction triggering analyses presented herein indicate that liquefaction will occur in numerous locations in the hydraulically placed fly ash and the alluvial sandy silt to silty sand soils. Assuming the analyzed SPT and CPT data are representative across the entire Dredge Cell, continuous liquefied zones that extend laterally should be anticipated at various elevations. Shear strength within these liquefied zones will drop to their residual strengths, which destabilizes the perimeter berm and the landfilled ash embankment slopes, as failure surfaces develop through these weakened zones. Therefore, design of the Dredge Cell closure plan should consider the scenario that the hydraulically placed fly ash and the alluvial sandy silt to silty sand soils have liquefied.

The screening analyses on the alluvial lean clay soil indicate that about 50 percent of the lean clay is susceptible to significant strength loss or liquefaction in earthquake events. In the design analyses for the dredge cell closure, the lean clay was assumed to be non-liquefiable and its post-earthquake strength was taken at 80 percent of its static,

undrained strength. In consideration of the relatively thin clay layer and the thick liquefied ash and silt/sand soils above and below the clay layer, the assumption of non-liquefiable clay does not appear to have a significant effect on the design.

The liquefaction triggering analyses were carried out using the "state-of-practice" NCEER method as presented in this report. In consideration of the unique site conditions at the Kingston Dredge Cell, some limitations associated with the analysis are briefly discussed below.

Equations for calculating the cyclic resistance ratio (*CRR*) based on SPT and CPT data (Eqn. 1.5 and Eqn. 1.14) were developed from empirical evaluations of field observations and field and laboratory tests on natural soils. The hydraulically placed fly ash at the Kingston site is not a natural soil. Its resistance against liquefaction may differ from that of natural soils from which Eqn. 1.5 and Eqn. 1.14 were developed.

Correlations for fines content correction based on CPT data (Eqn. 1.12 and Eqn. 1.13) were developed from natural soils with fines content generally less than about 35%. The corrections are not well defined for pure silts. For the Kingston site, the existing hydraulically placed fly ash contains fines content of up to 100%, which may make Eqn. 1.12 and Eqn. 1.13 questionable or invalid. However, without more definitive correlations on the ash material, it was considered appropriate to use these equations along with the additional criteria as discussed in Section 1.5.2.

The correction factor K_α was used in the analysis to account for the effects of static shear stresses on the *CRR*; however, K_α is not well defined. Limitations associated with K_α are discussed in Section 1.6.3. In addition, the final geometries of the closure plan have not been fully established at the time of this triggering analysis, locations of the analyzed borings with respect to the proposed perimeter berm were only approximate, adding uncertainty to the a values, which were calculated based on a typical cross section and the four defined profiles as described in Section 1.6.3.

The earthquake induced shear stresses were calculated using the *ProShake* program as discussed in the ground response analysis report. Shear wave velocities were assigned to the existing hydraulically placed ash, lean clay, sandy silt to silty sand, and the weathered shale based on the field measurements. The scattered shear wave velocity data introduced uncertainties to the calculated cyclic shear stresses. In addition, effects of the landfilled ash embankment and the perimeter berm on the soil shear wave velocities were not considered in the analyses, adding more uncertainties to the calculated cyclic shear stresses.

Despite the above mentioned limitations, the analyses presented in this report are considered reasonable. The results of the analyses provide valuable inputs for the closure plan design. The perimeter berm needs to be designed to meet all the required stability and deformation criteria considering the scenario that the existing hydraulically placed ash and the alluvial silt/sand soils have liquefied.

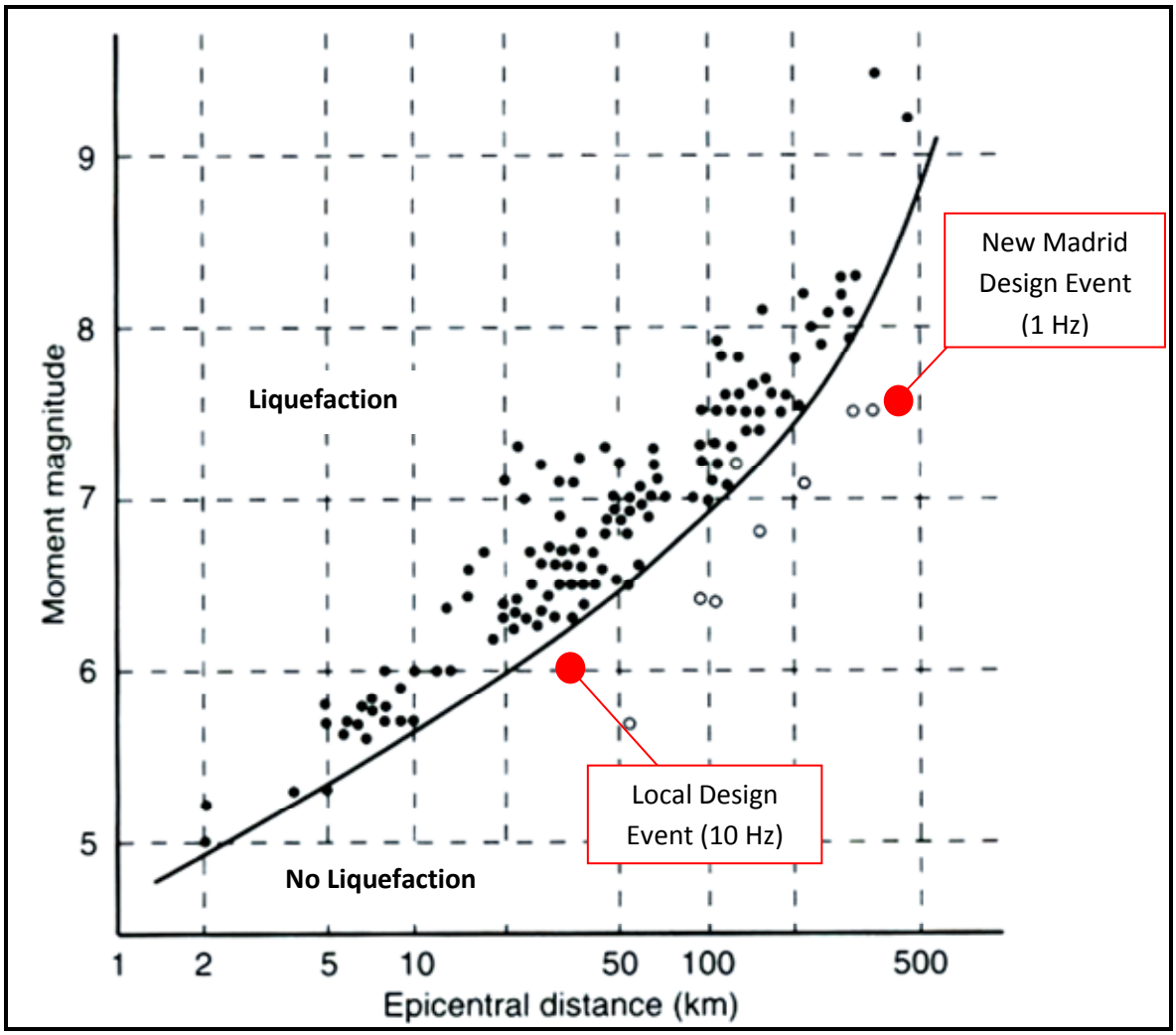

Figure 1.1 – Maximum Epicentral Distance to Observed Liquefaction Events in Shallow (Focal Depth < 50 km) Earthquakes (Kramer 1996, from Ambraseys 1988)

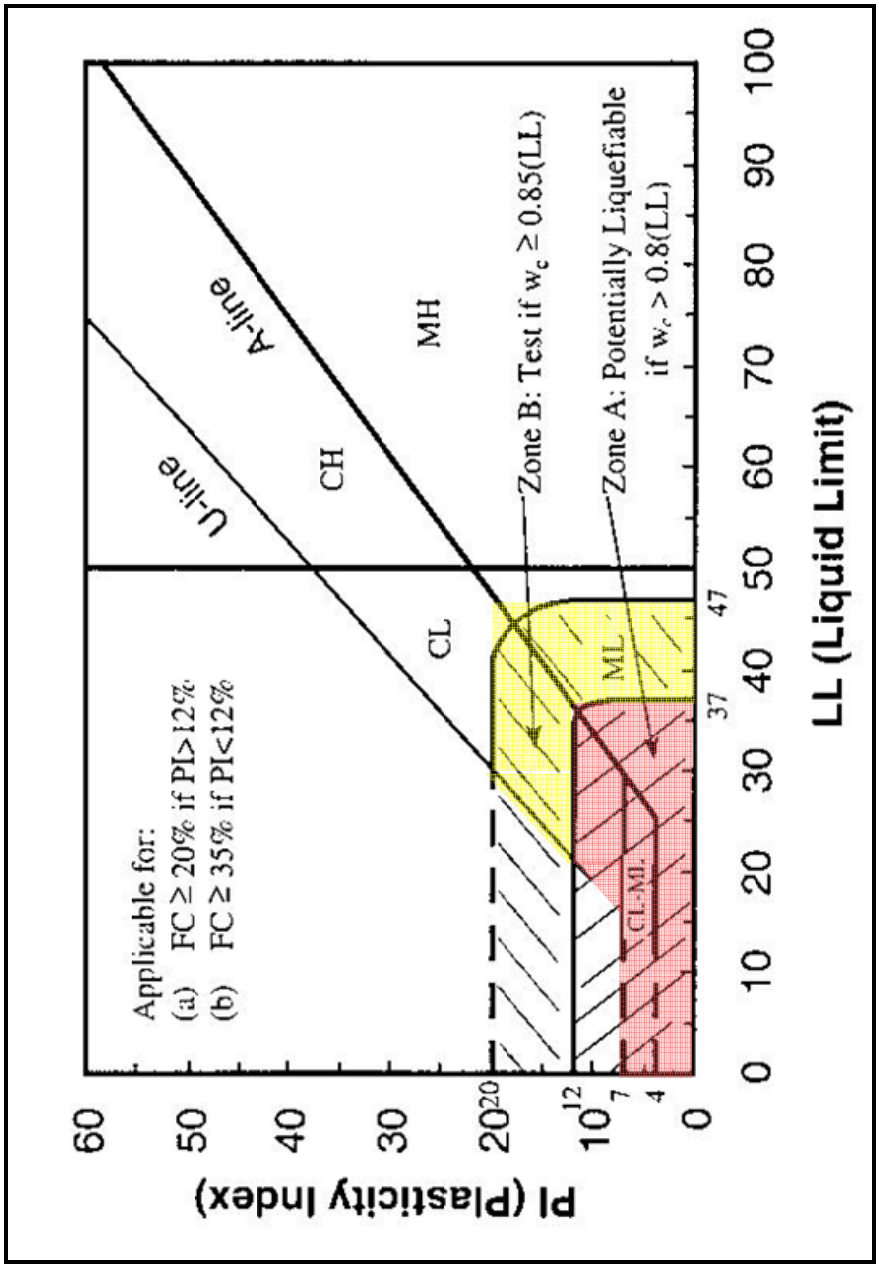

Figure 1.2 – Criteria for Assessing Liquefaction in Fine-Grained Soils (after Seed et al. 2003)

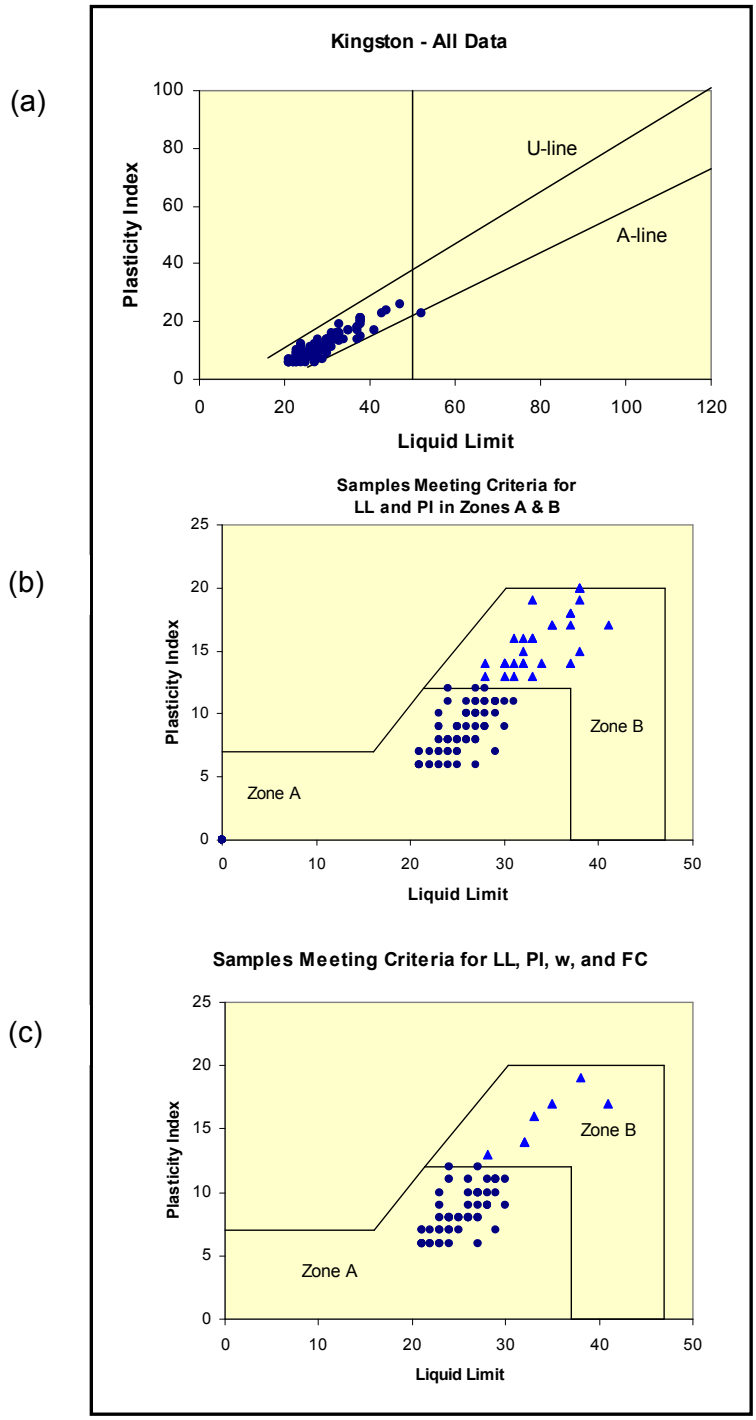

Figure 1.3 – Evaluation of Fine-Grained Soils for Potential Liquefaction

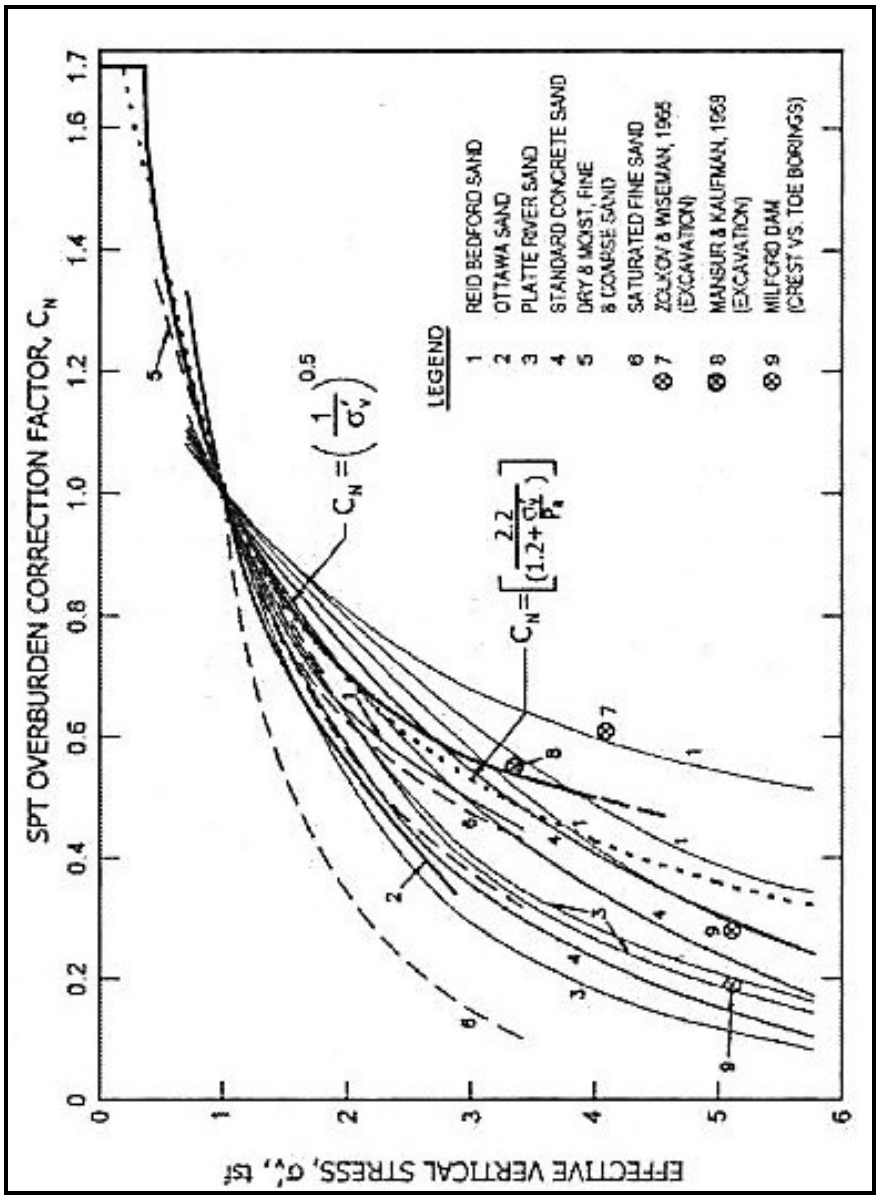

Figure 1.4 – Correction Factor for Overburden Pressure (Youd et al. 2001)

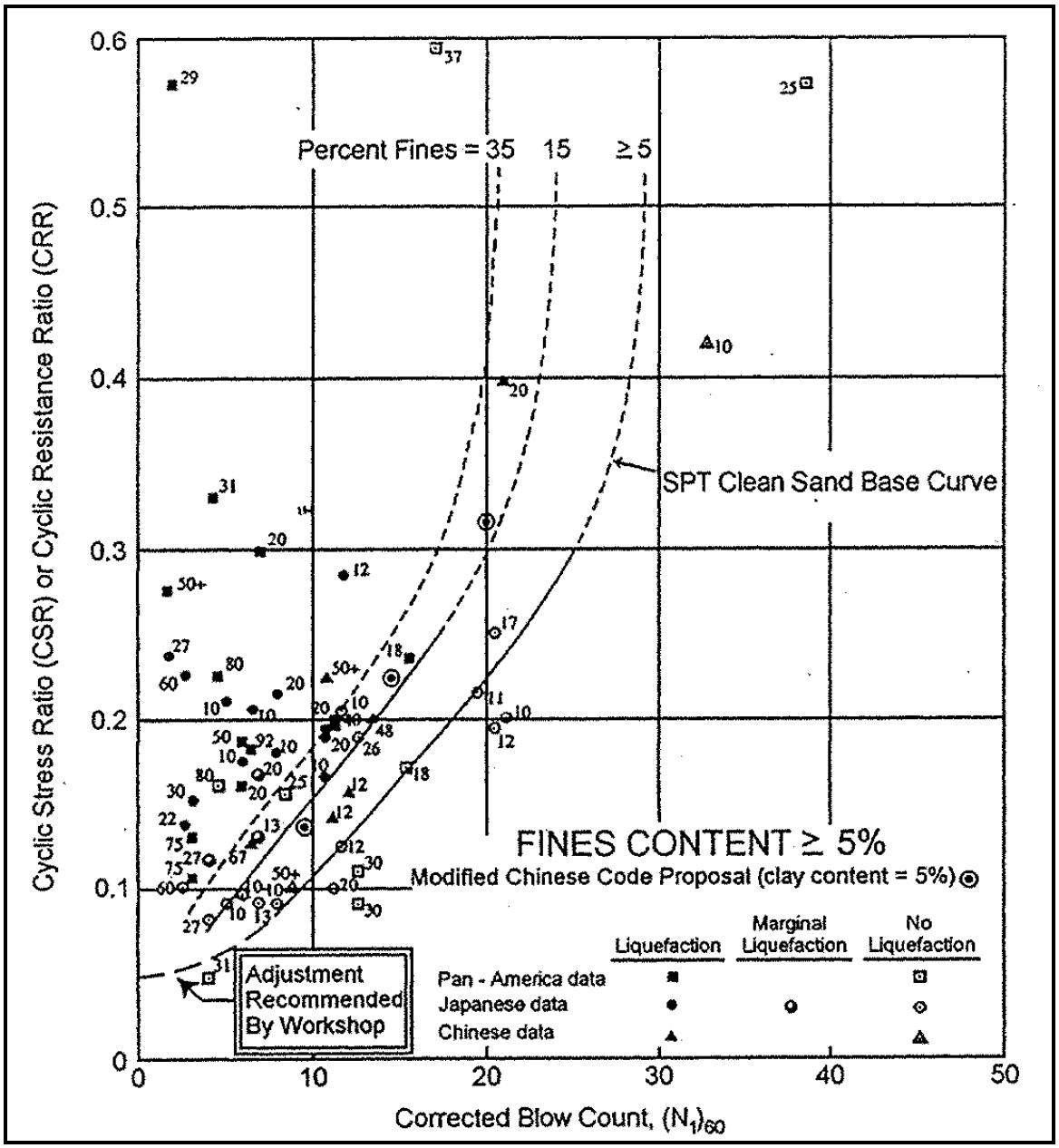

Figure 1.5 – Field Data and Empirical Relationship between Liquefaction Resistance and Corrected N_{SPT} (Youd et al. 2001)

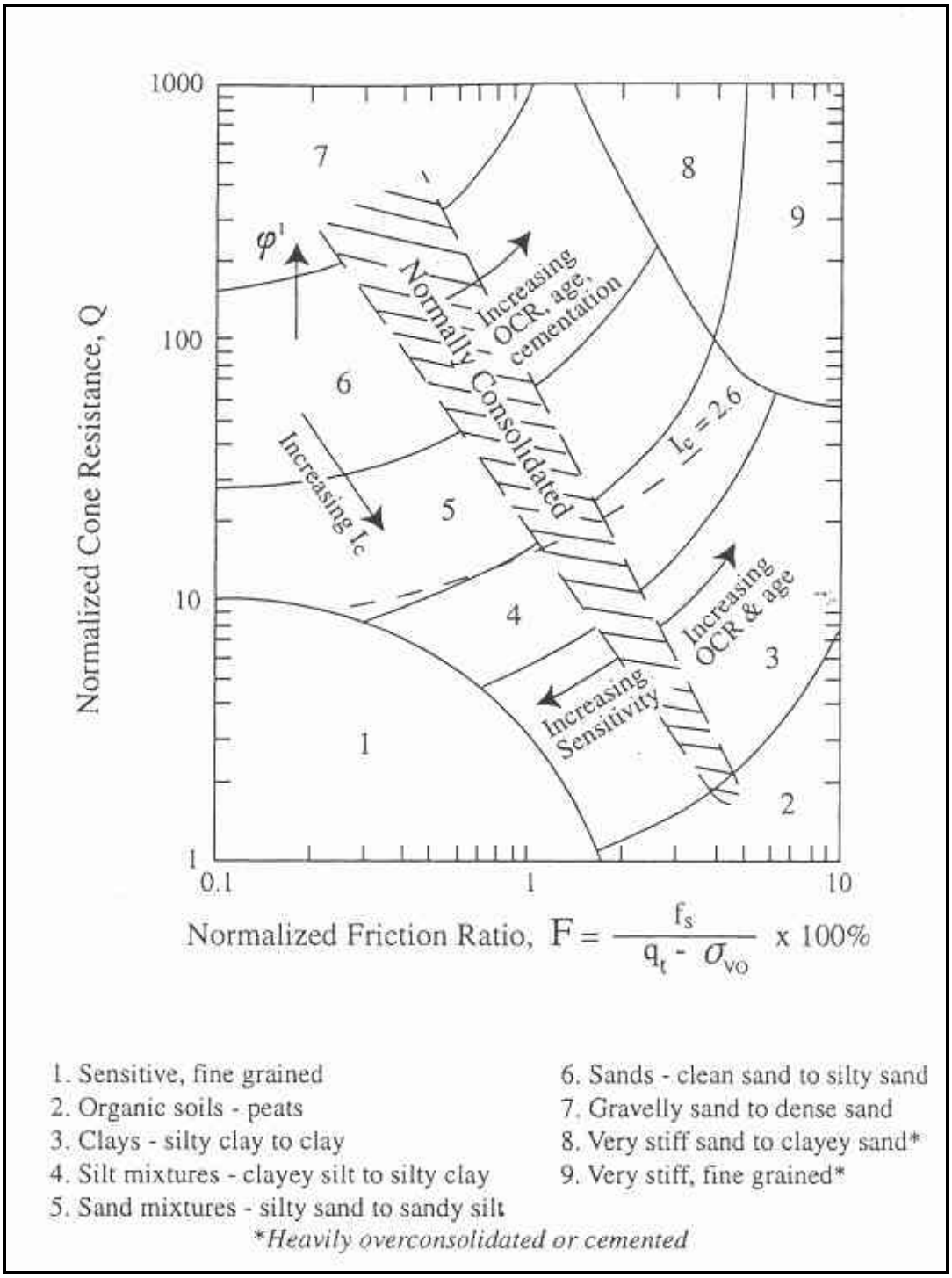

Figure 1.6 – Soil Behavior-Type Chart for Classifying Soils from CPT Data (Youd et al. 2001, after Robertson 1990)

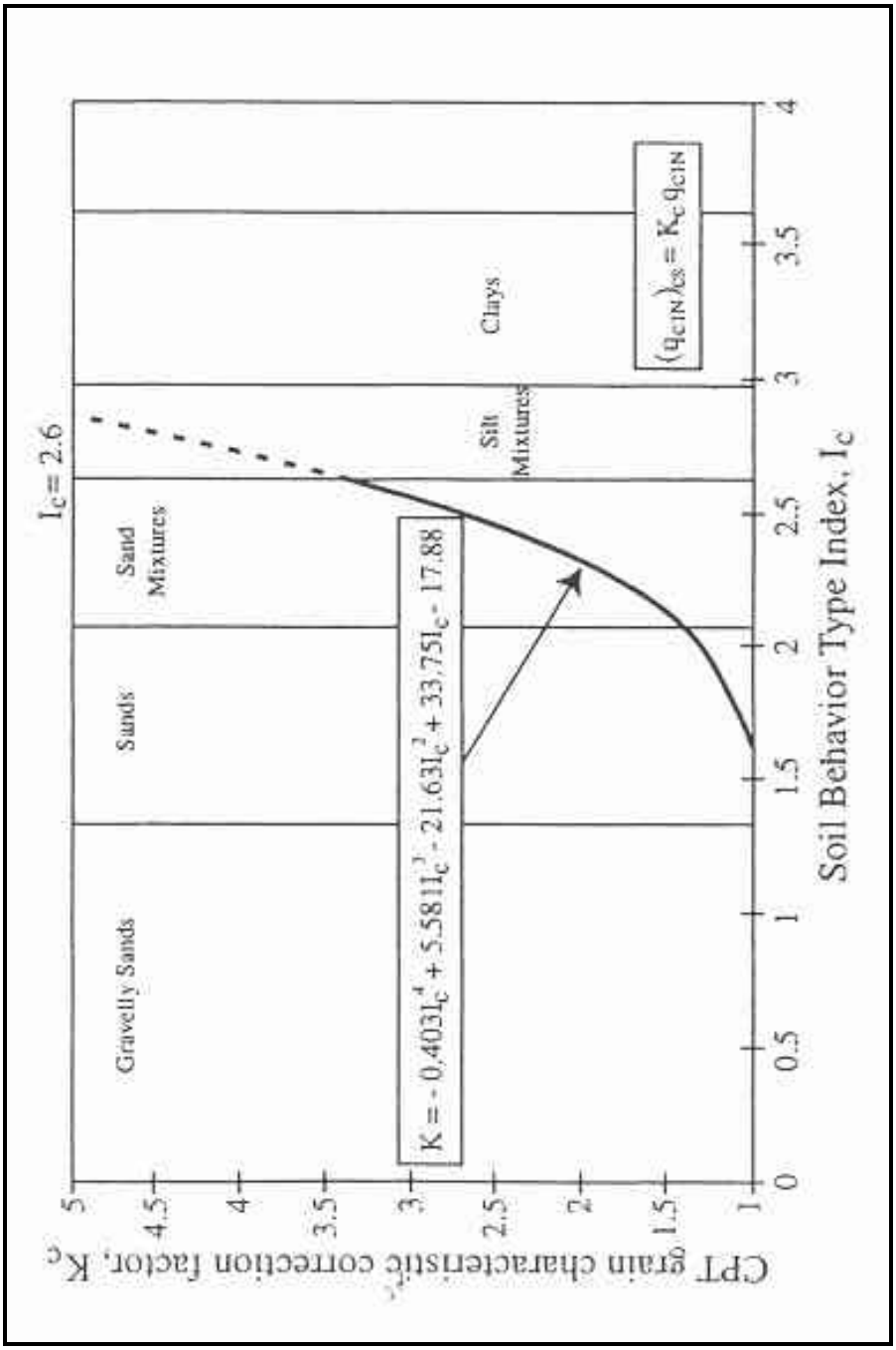

Figure 1.7 – Grain Size Correction Factor (K_c) for Determination of a Clean-Sand Equivalent CPT Tip Resistance (Youd et al. 2001, after Robertson and Wride 1998)

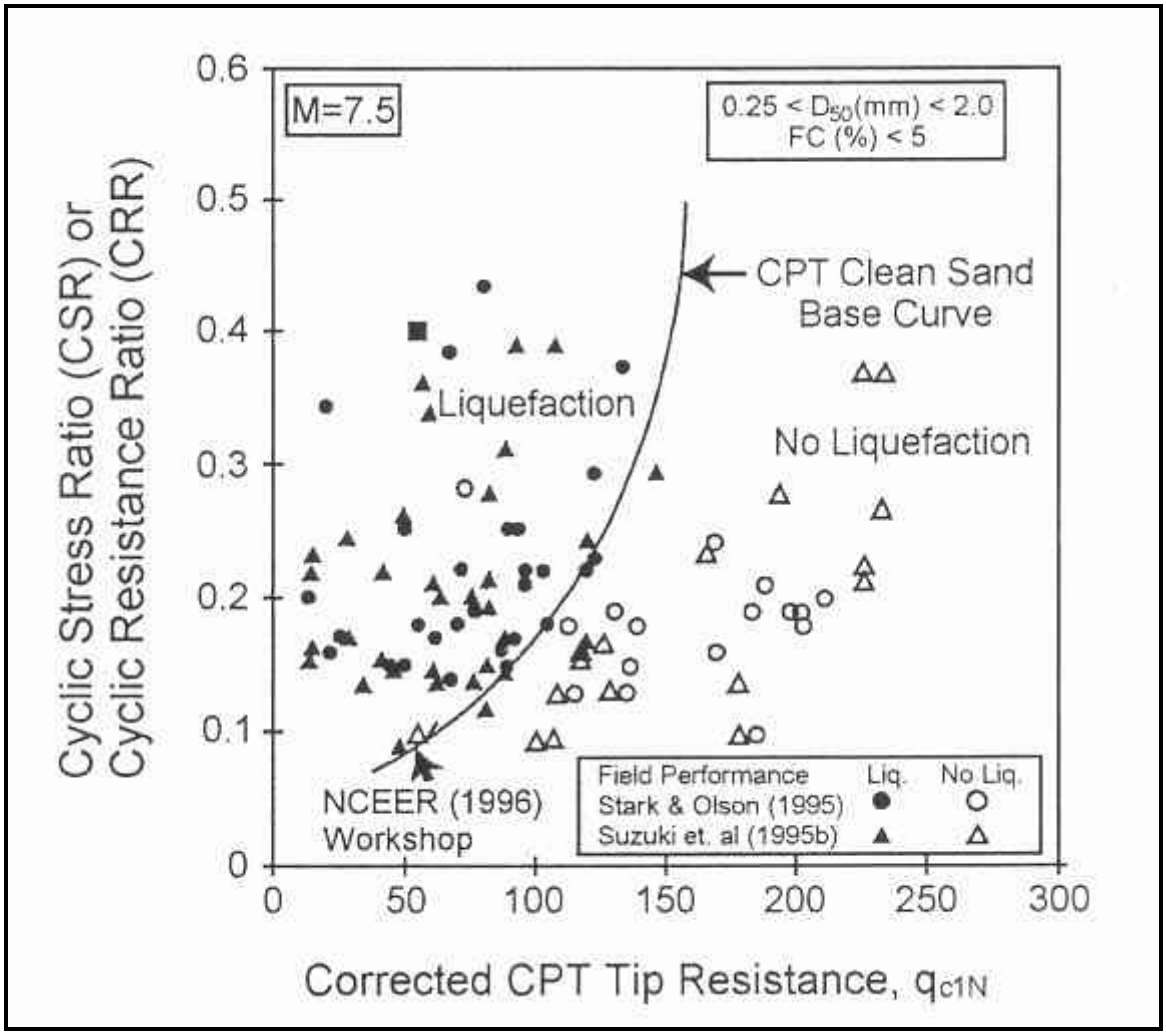

Figure 1.8 – Curve and Case History Data Relating Cone Penetration Resistance to Liquefaction Resistance (Youd et al. 2001, after Robertson and Wride 1998)

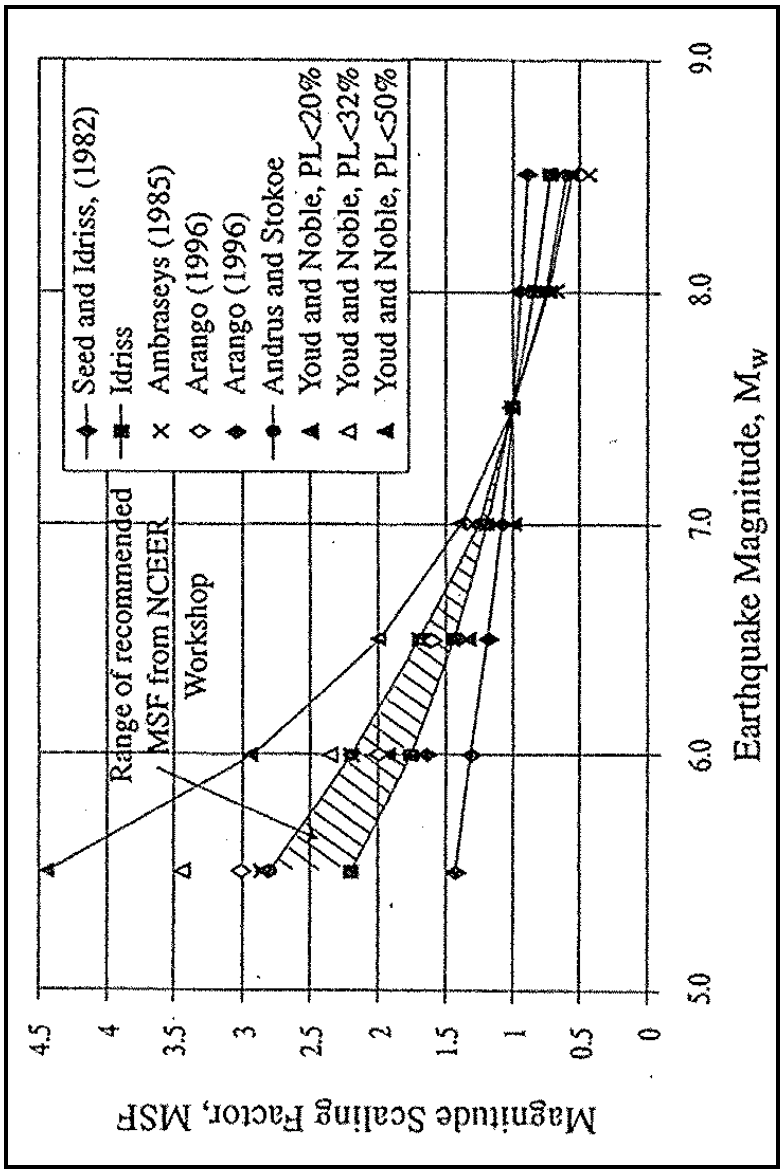

Figure 1.9 – *MSF* for Correcting *CRR* for Earthquake Magnitude (Youd et al. 2001)

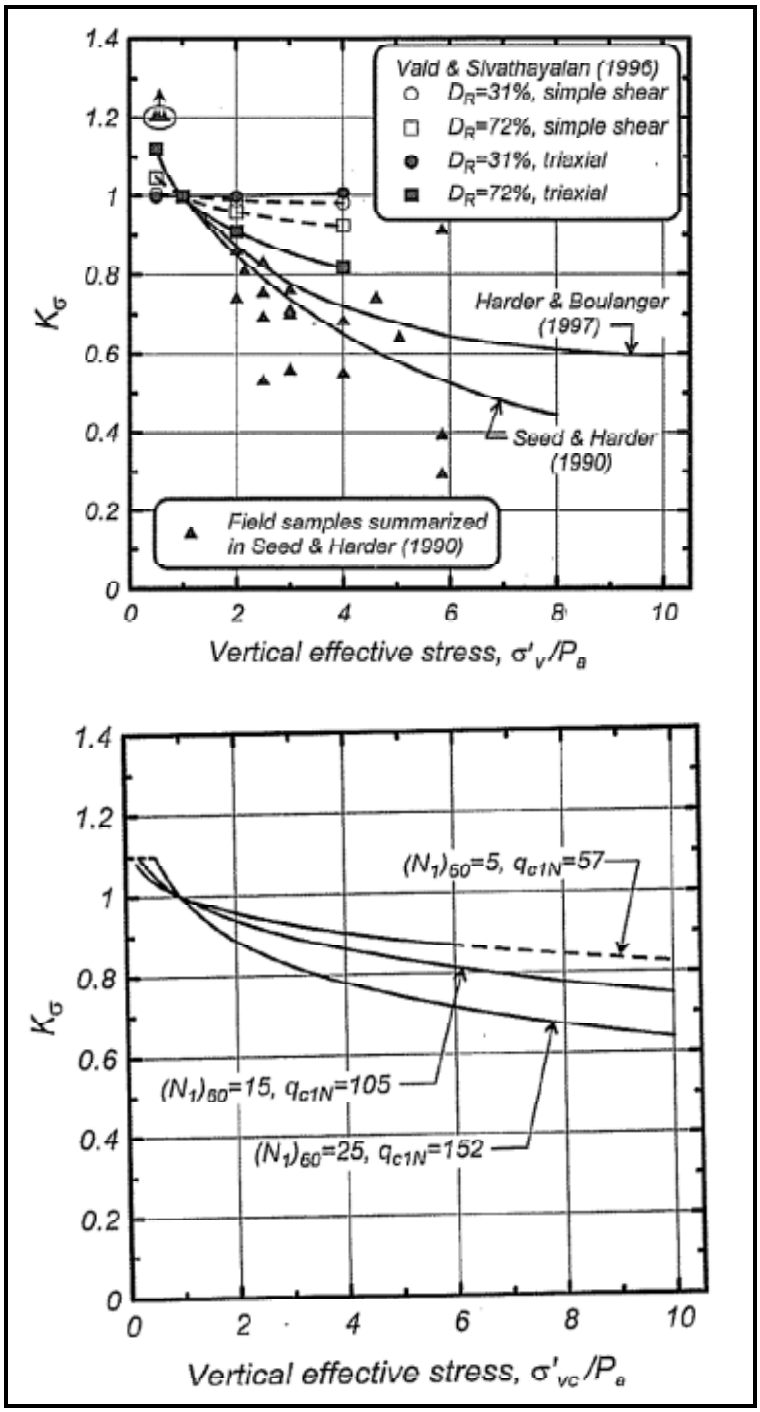

Figure 1.10 – K_σ Factor for Correcting *CRR* for Overburden Pressure (Example Data and Sample Curves from Idriss and Boulanger 2008)

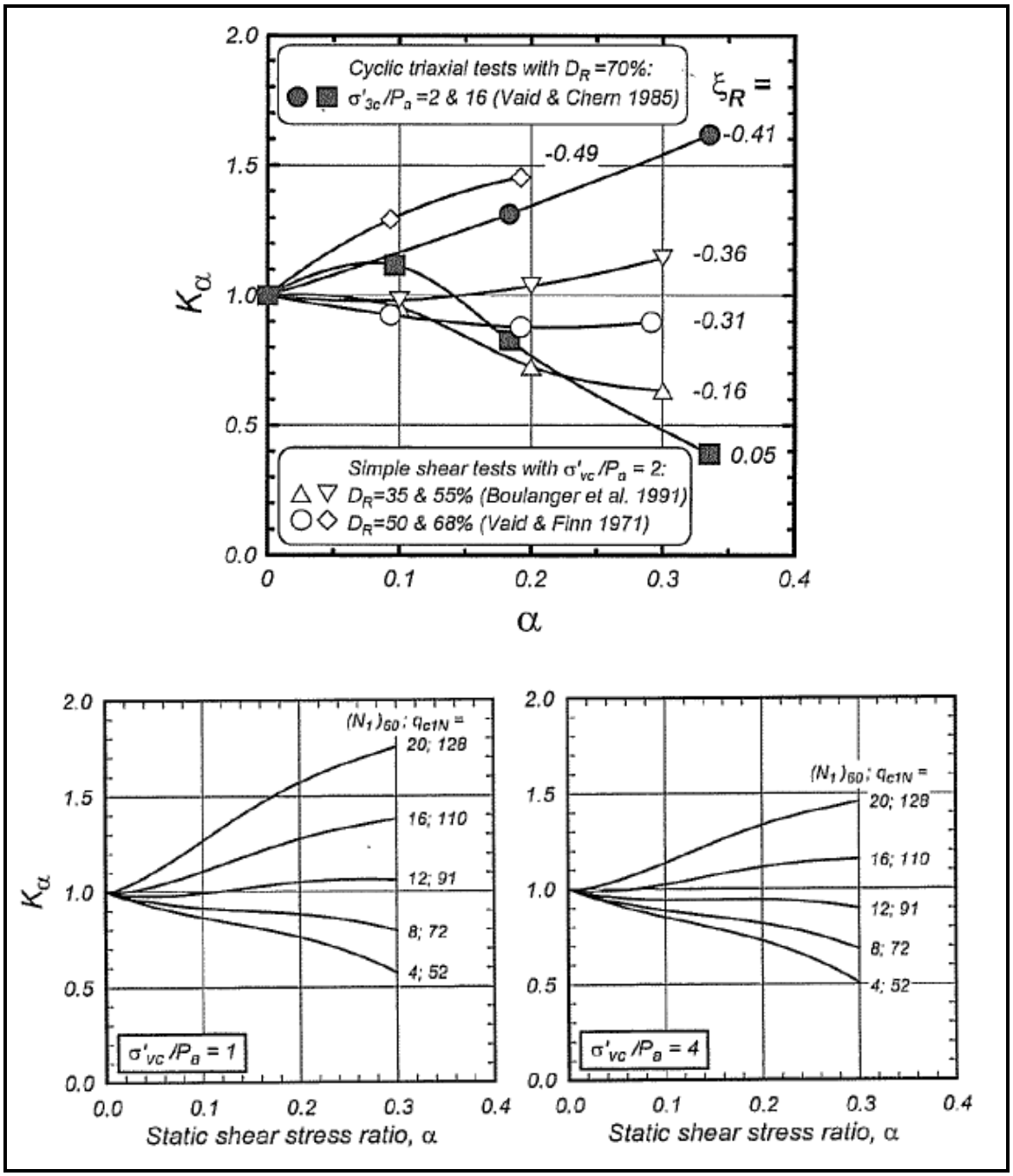

Figure 1.11 – K_α Factor for Correcting *CRR* for Static Driving Shear Stress (Example Data and Sample Curves from Idriss and Boulanger 2008)

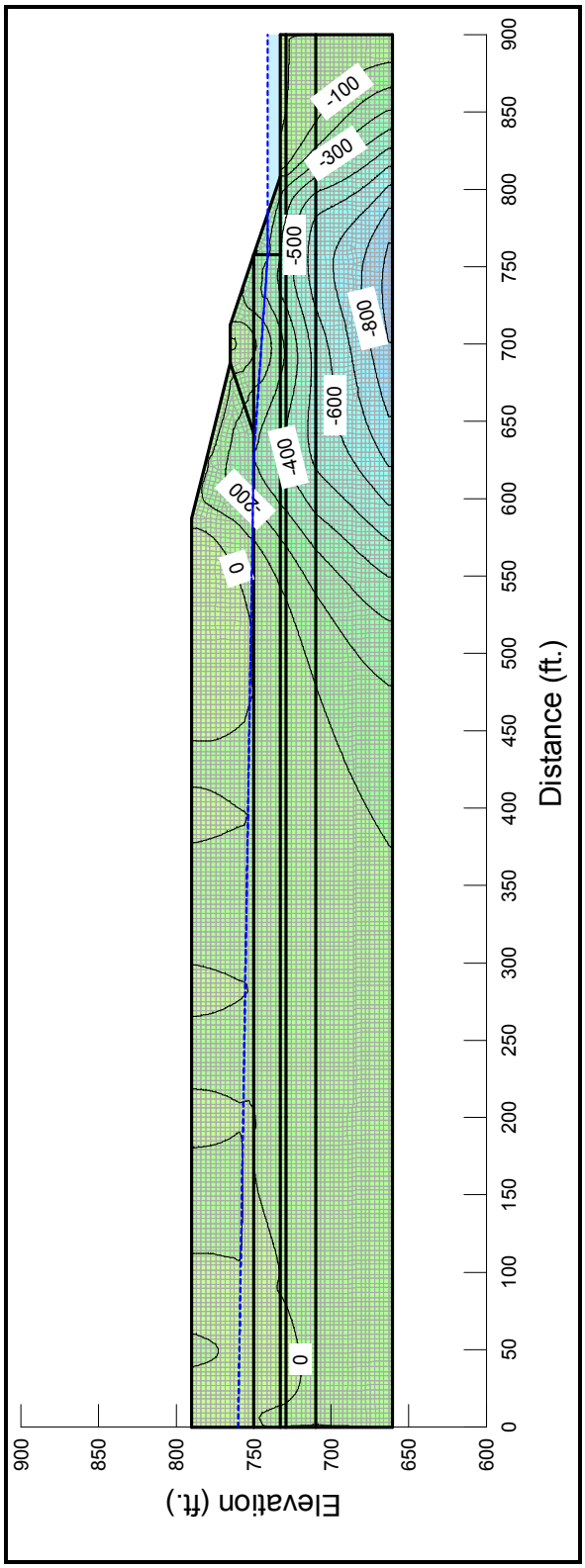

Figure 1.12 – Contours of Static Shear Stresses from SIGMA/W Analysis on a Typical Cross Section

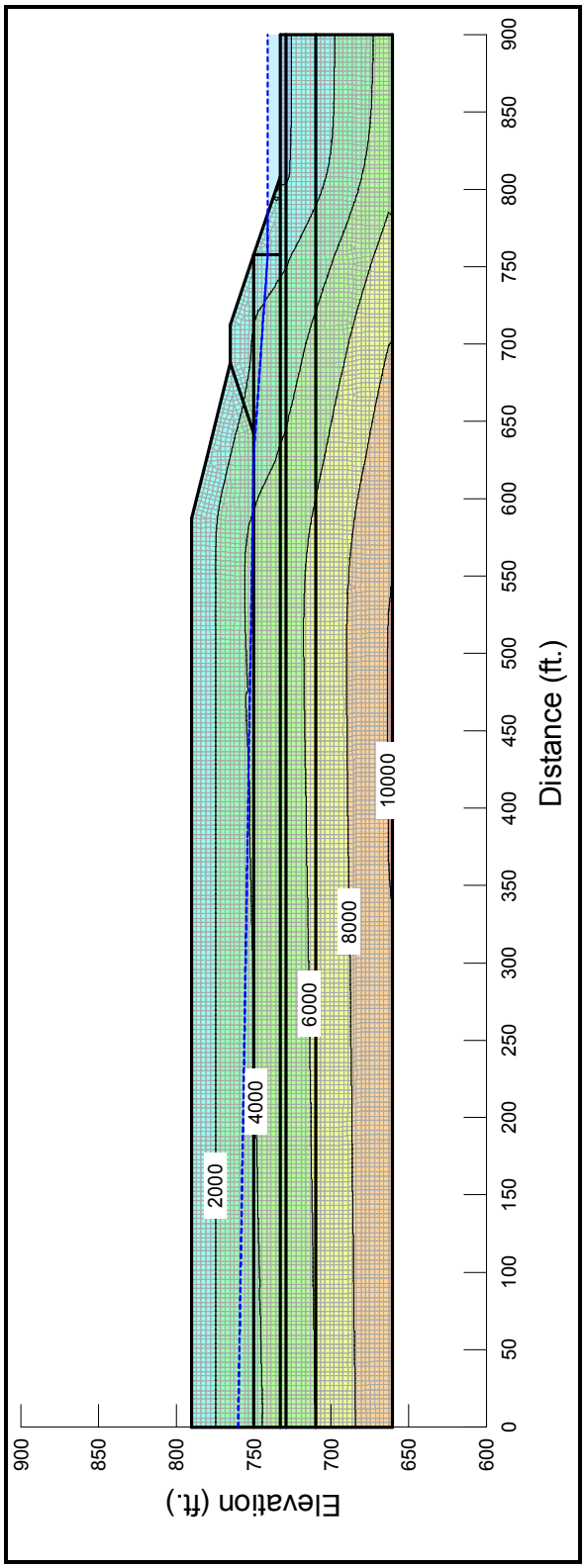

Figure 1.13 – Contours of Vertical Effective Stresses from SIGMA/W Analysis on a Typical Cross Section

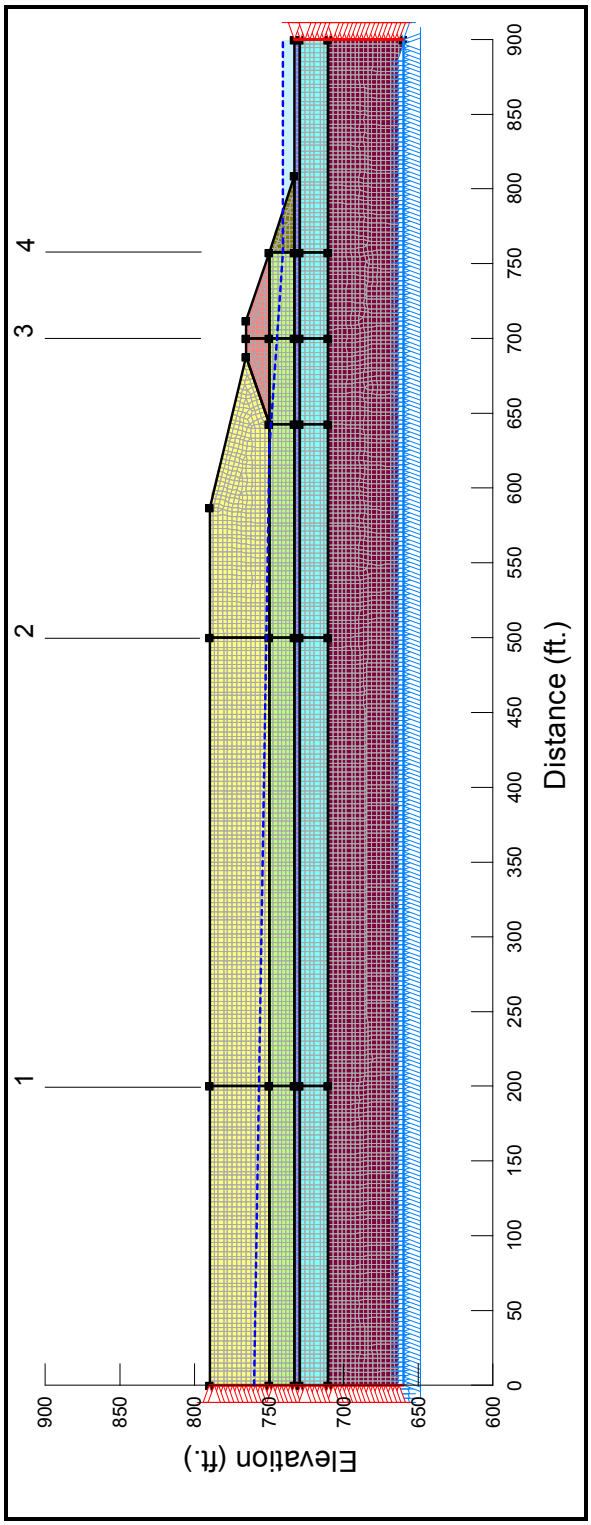

Figure 1.14 – Locations of Four Defined Profiles for Calculating α

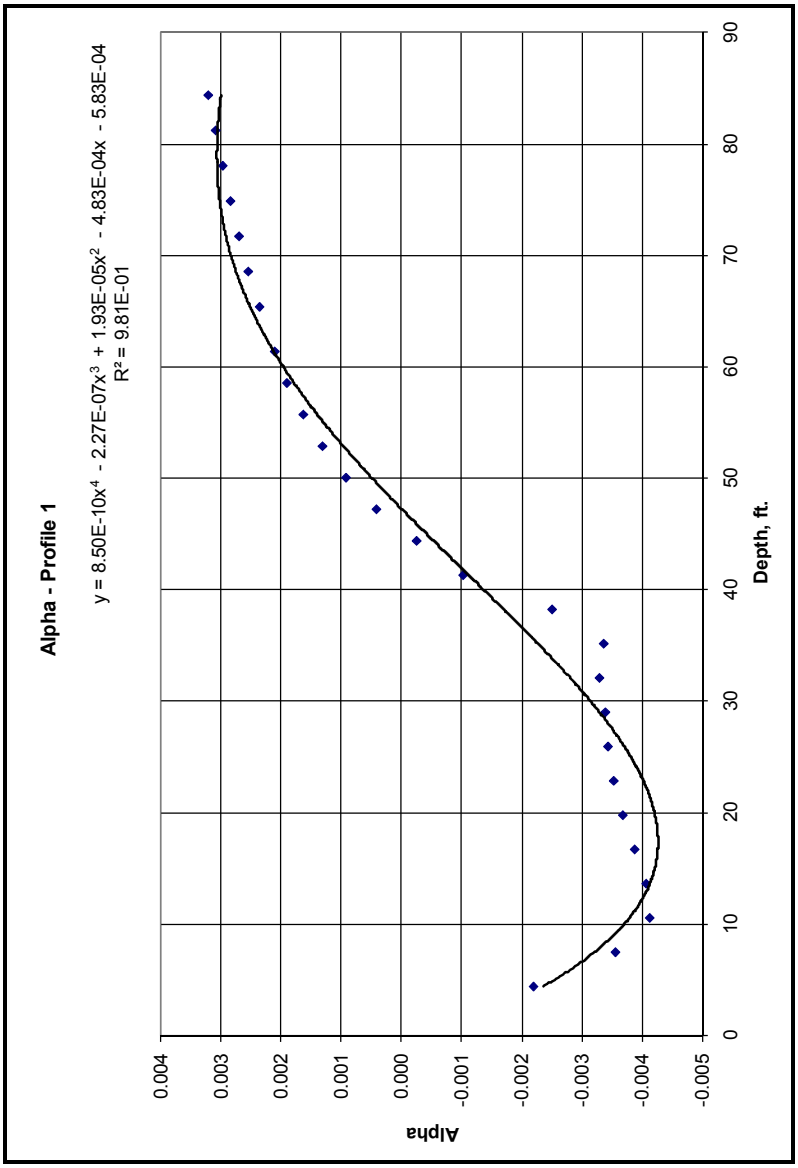

Figure 1.15 – Curve Fit Defining α vs. Depth (Profile 1)

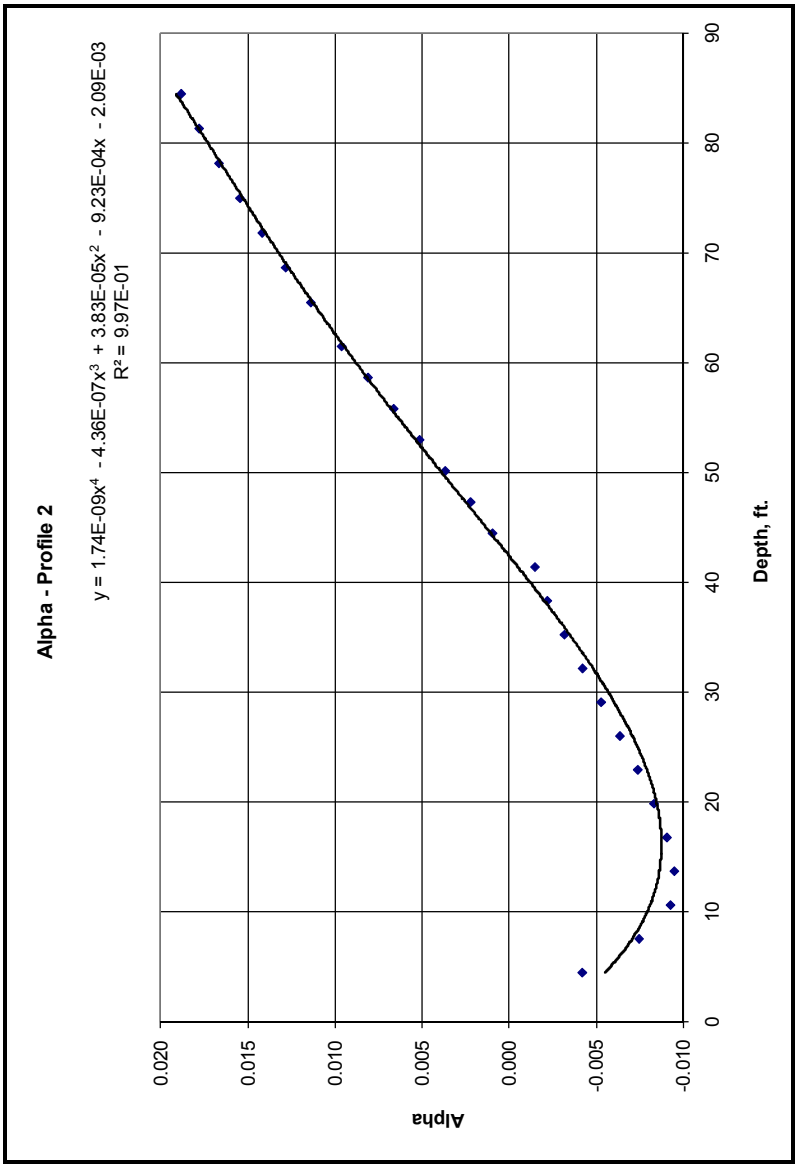

Figure 1.16 – Curve Fit Defining α vs. Depth (Profile 2)

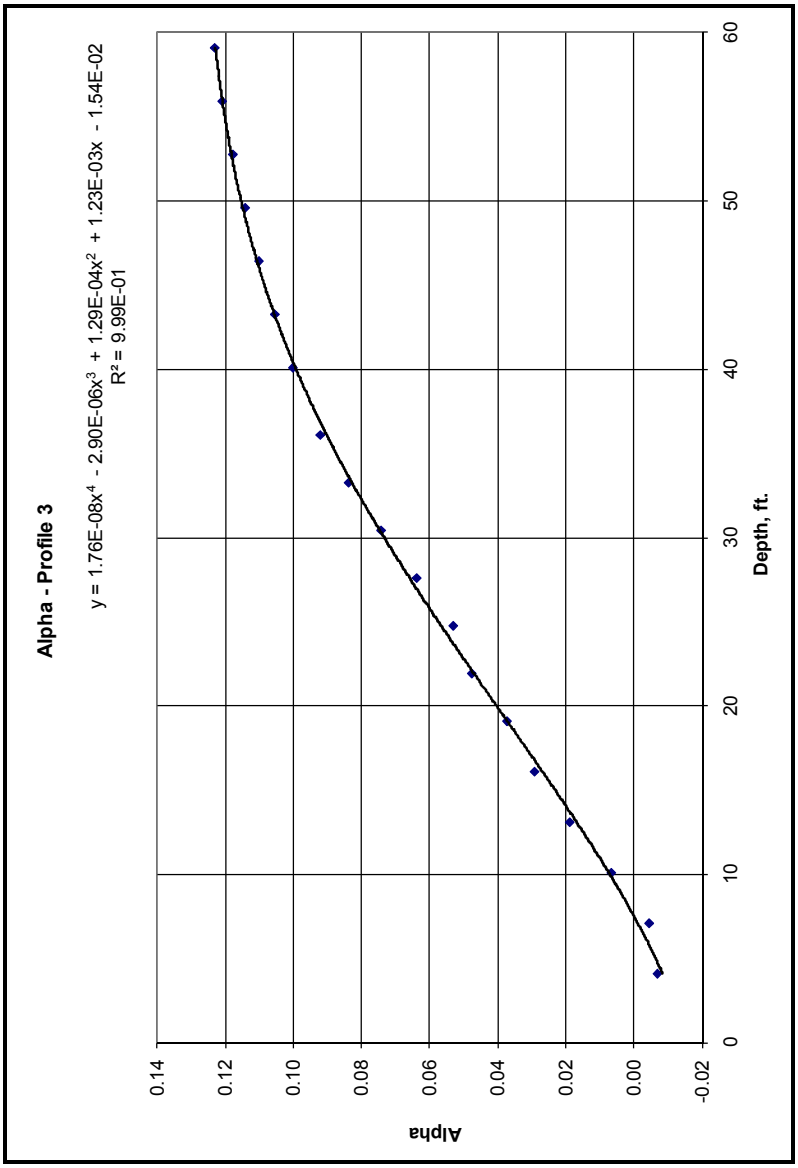

Figure 1.17 – Curve Fit Defining α vs. Depth (Profile 3)

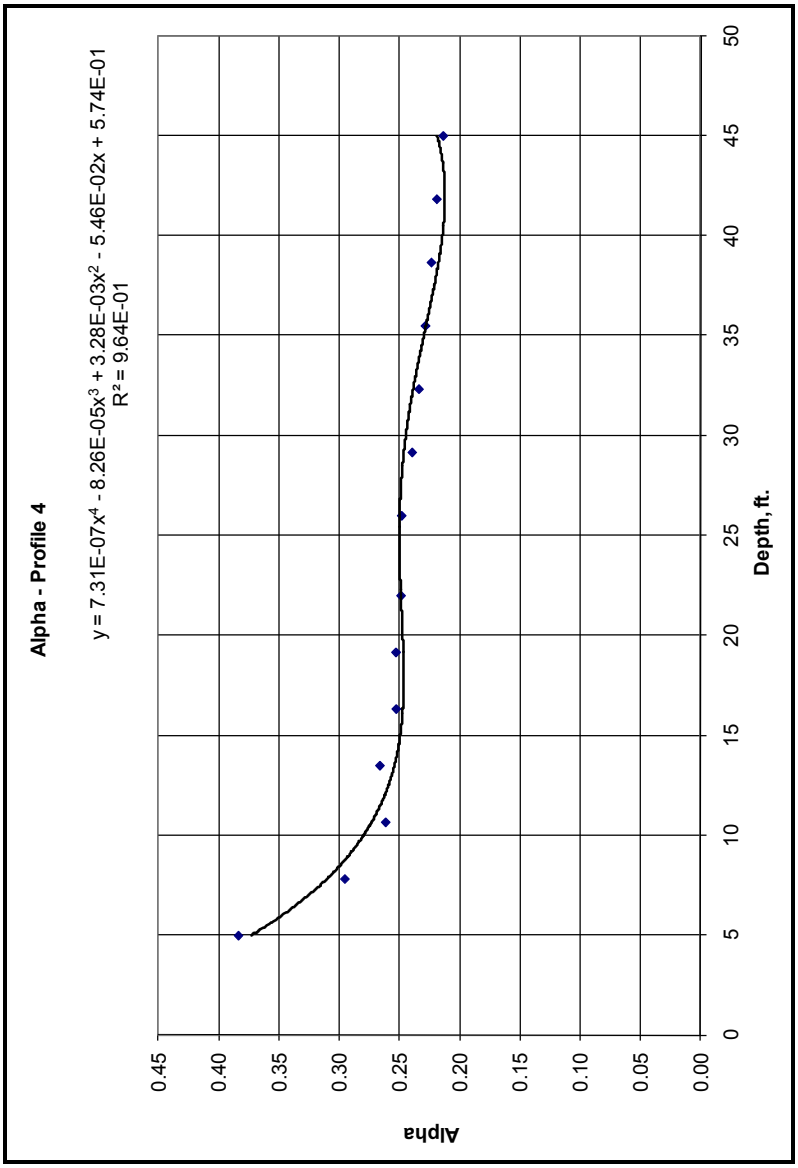

Figure 1.18 – Curve Fit Defining α vs. Depth (Profile 4)

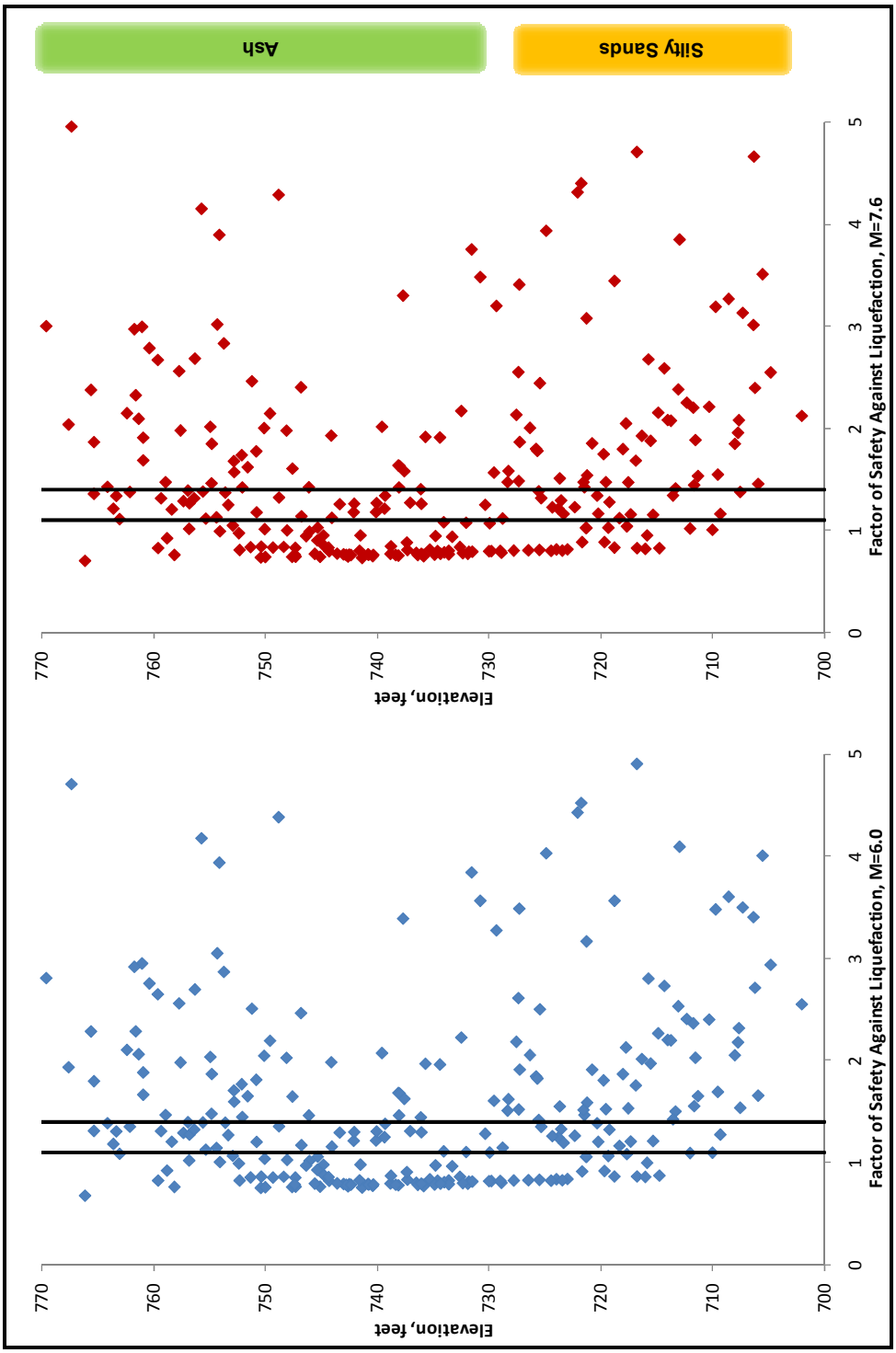

Figure 1.19 – Calculated Factors of Safety against Liquefaction (100-Series SPT Data)

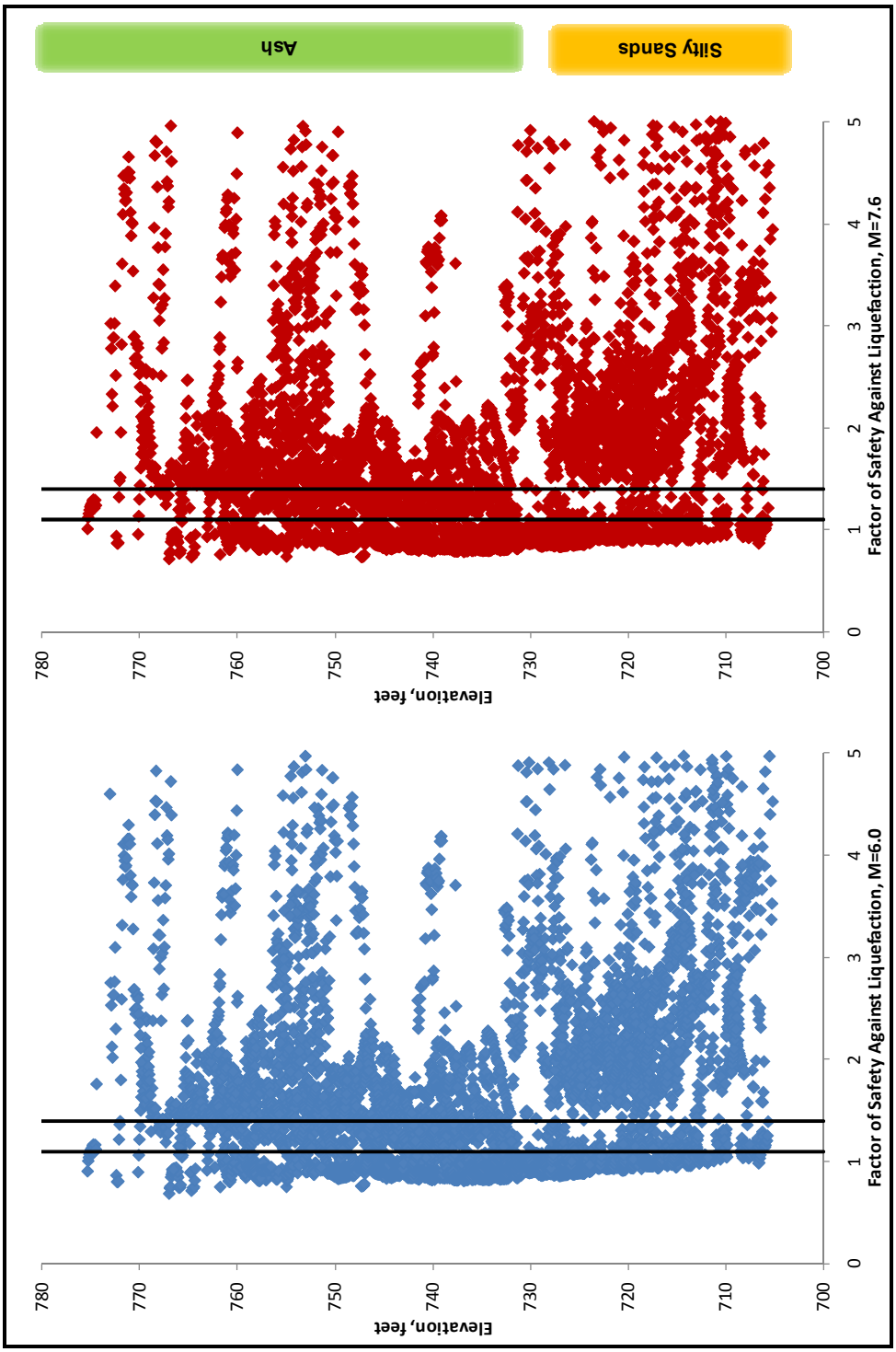

Figure 1.20 – Calculated Factors of Safety against Liquefaction (100-Series CPT Data)

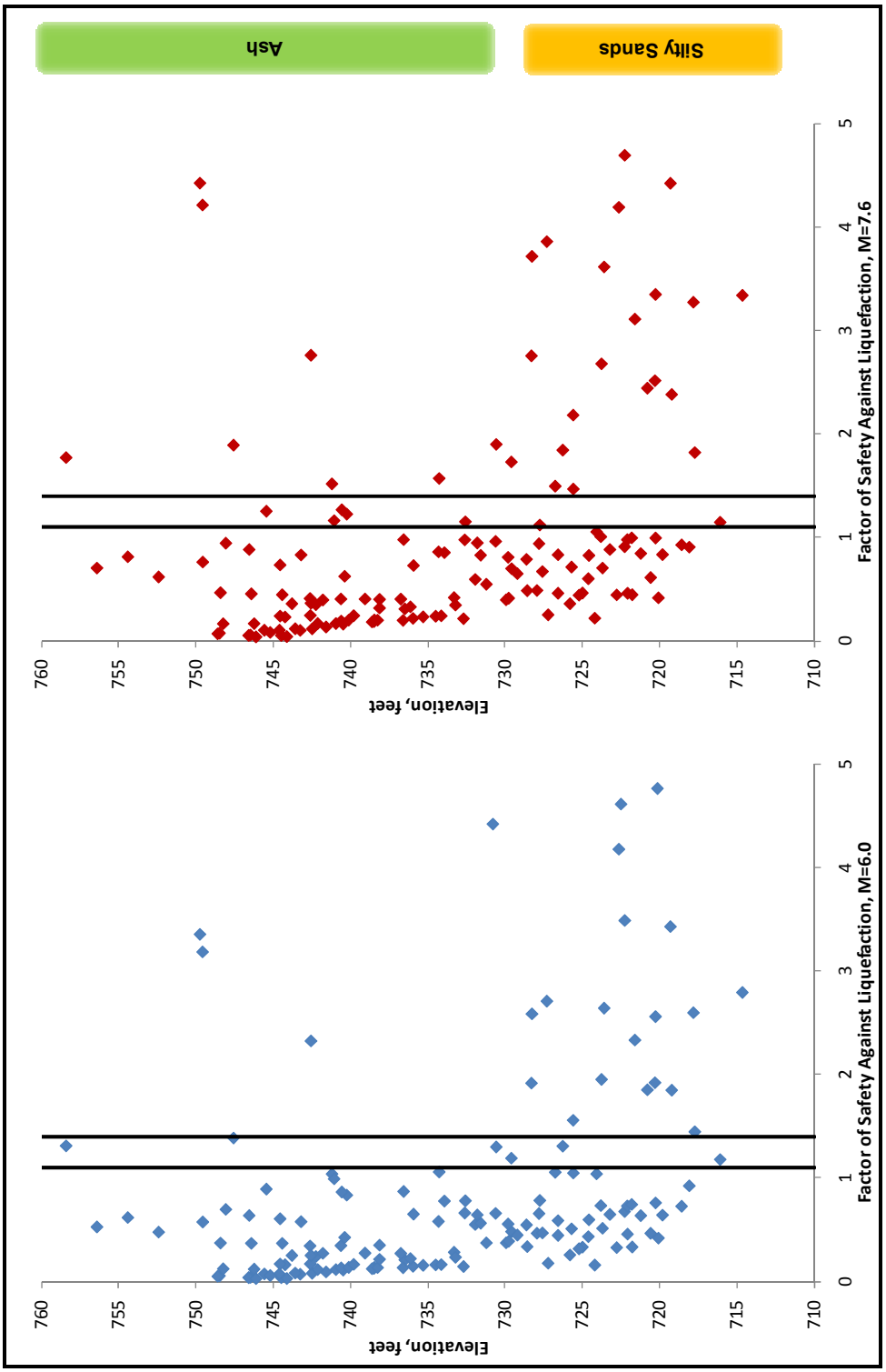

Figure 1.21 – Calculated Factors of Safety against Liquefaction (200-Series SPT Data)

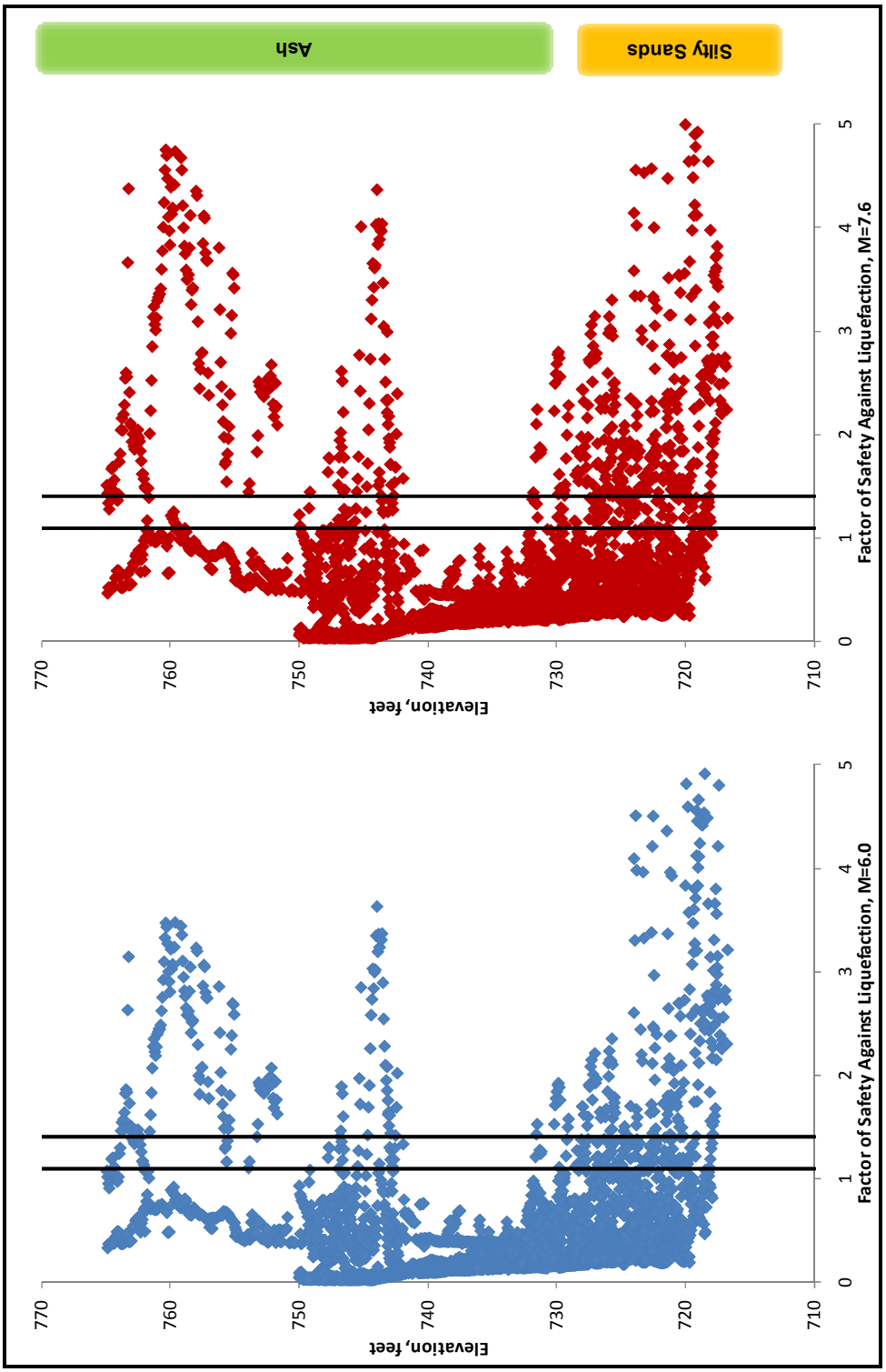

Figure 1.22 – Calculated Factors of Safety against Liquefaction (200-Series CPT Data)

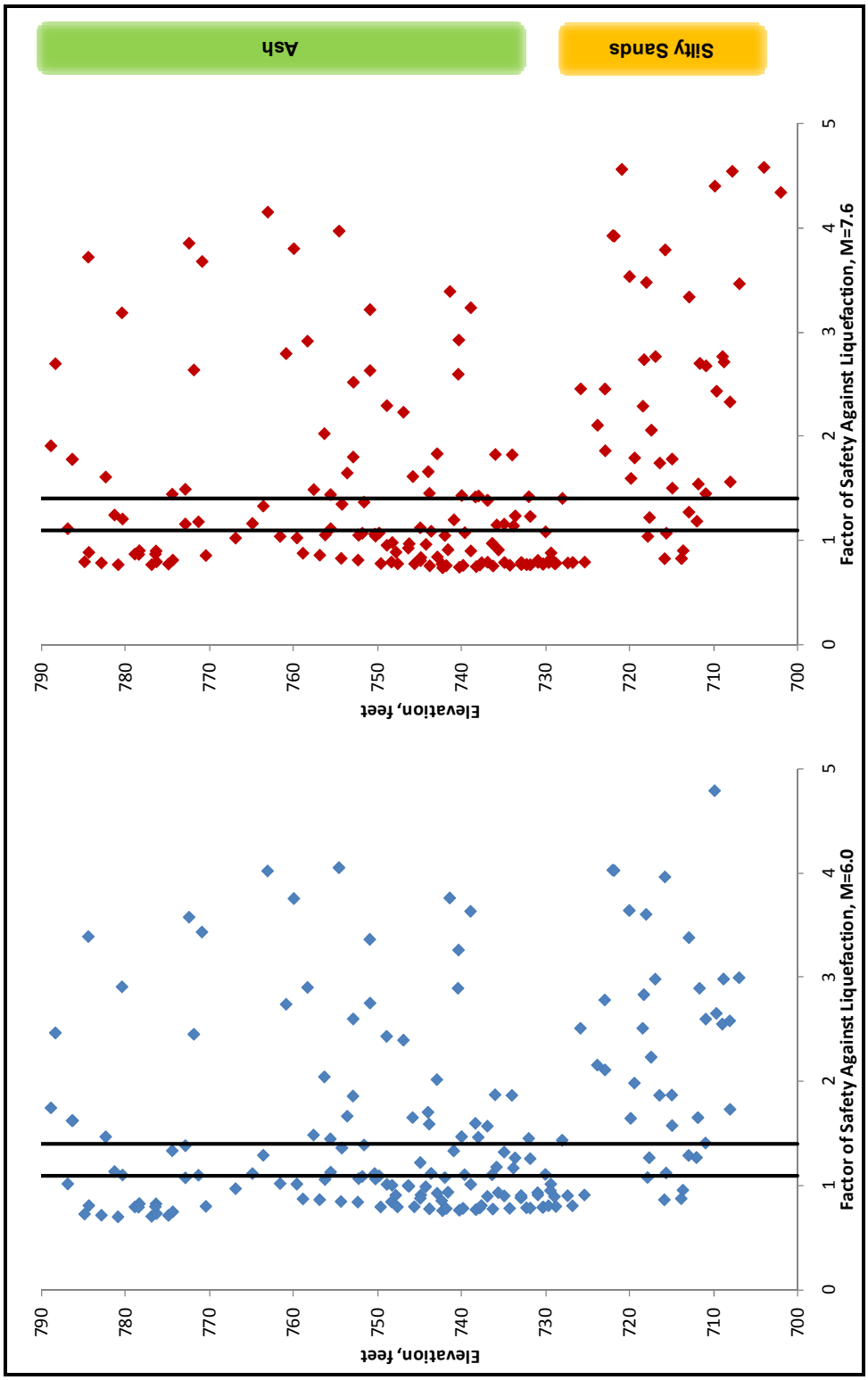

Figure 1.23 – Calculated Factors of Safety against Liquefaction (300- and 500-Series SPT Data)

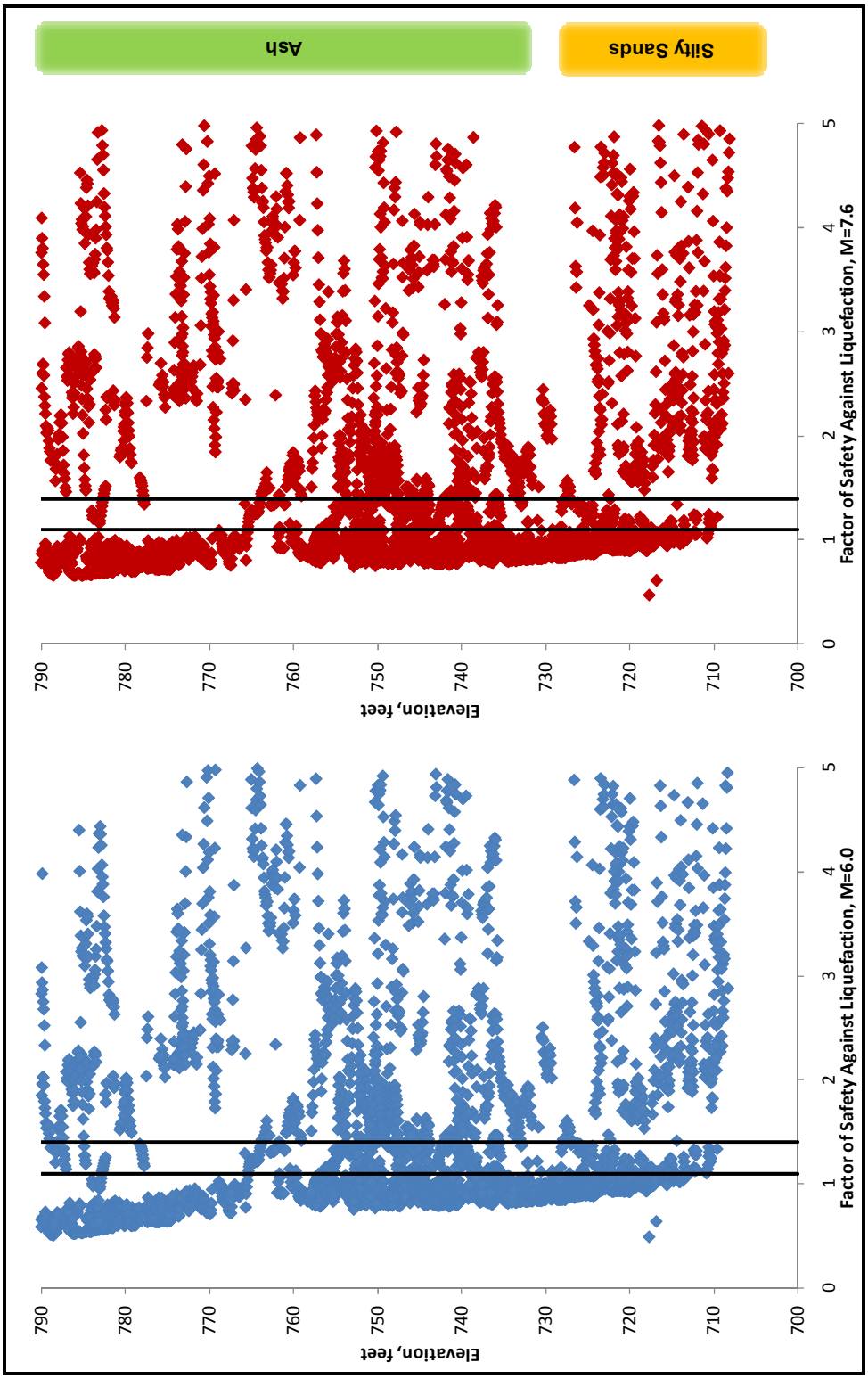

Figure 1.24 – Calculated Factors of Safety against Liquefaction (300- and 500-Series CPT Data)

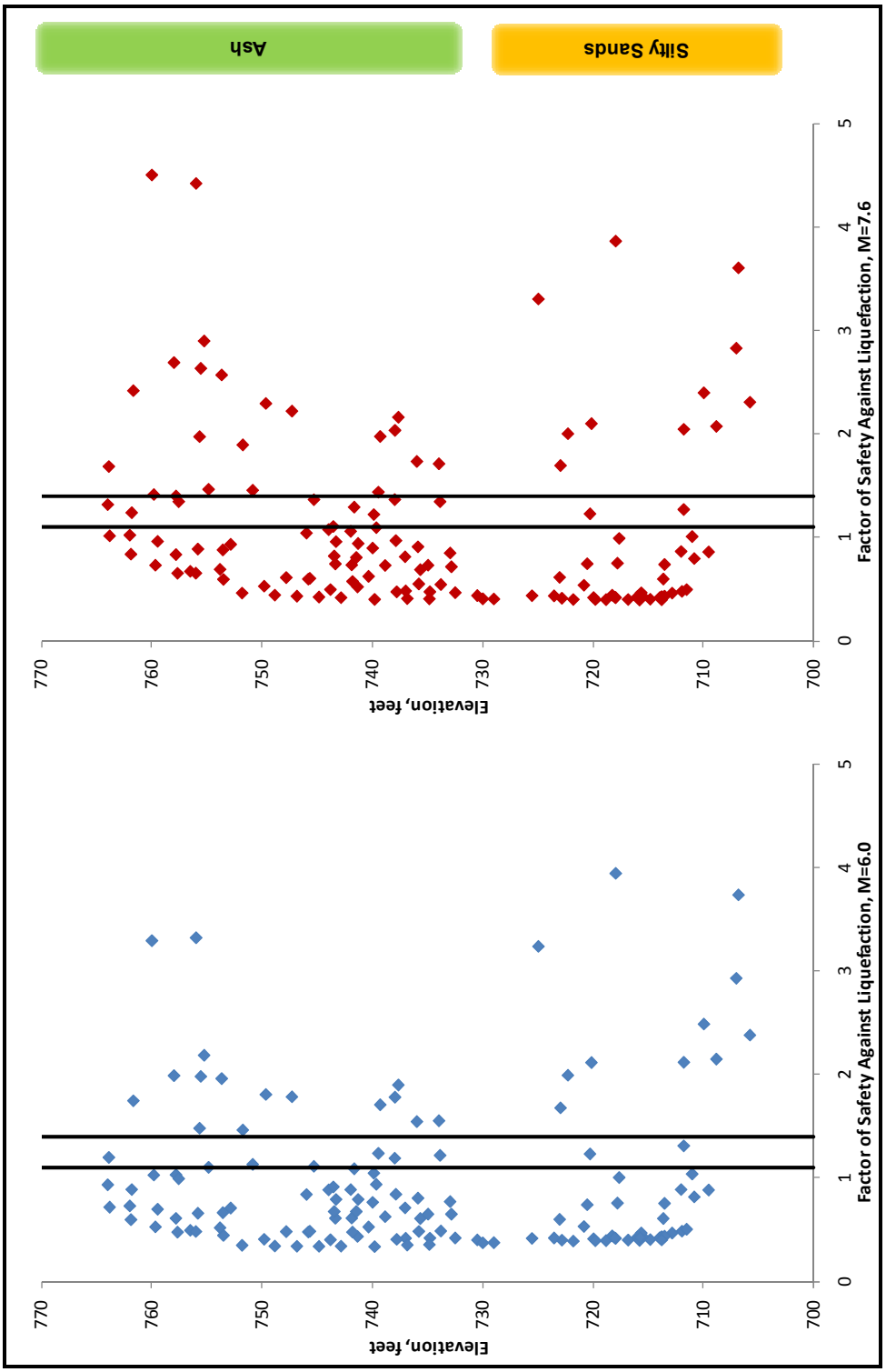

Figure 1.25 – Calculated Factors of Safety against Liquefaction (400-Series SPT Data)

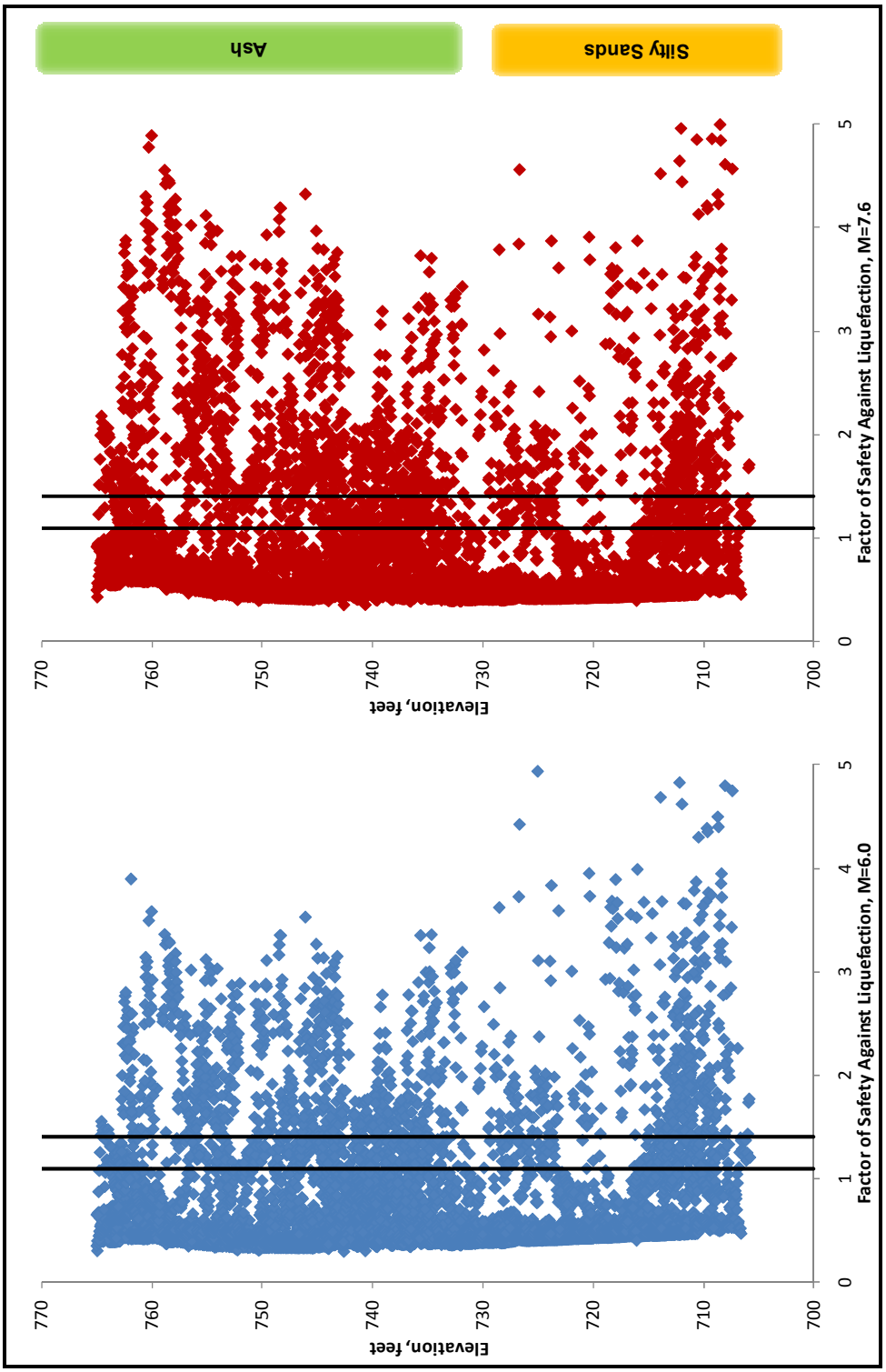

Figure 1.26 – Calculated Factors of Safety against Liquefaction (400-Series CPT Data)

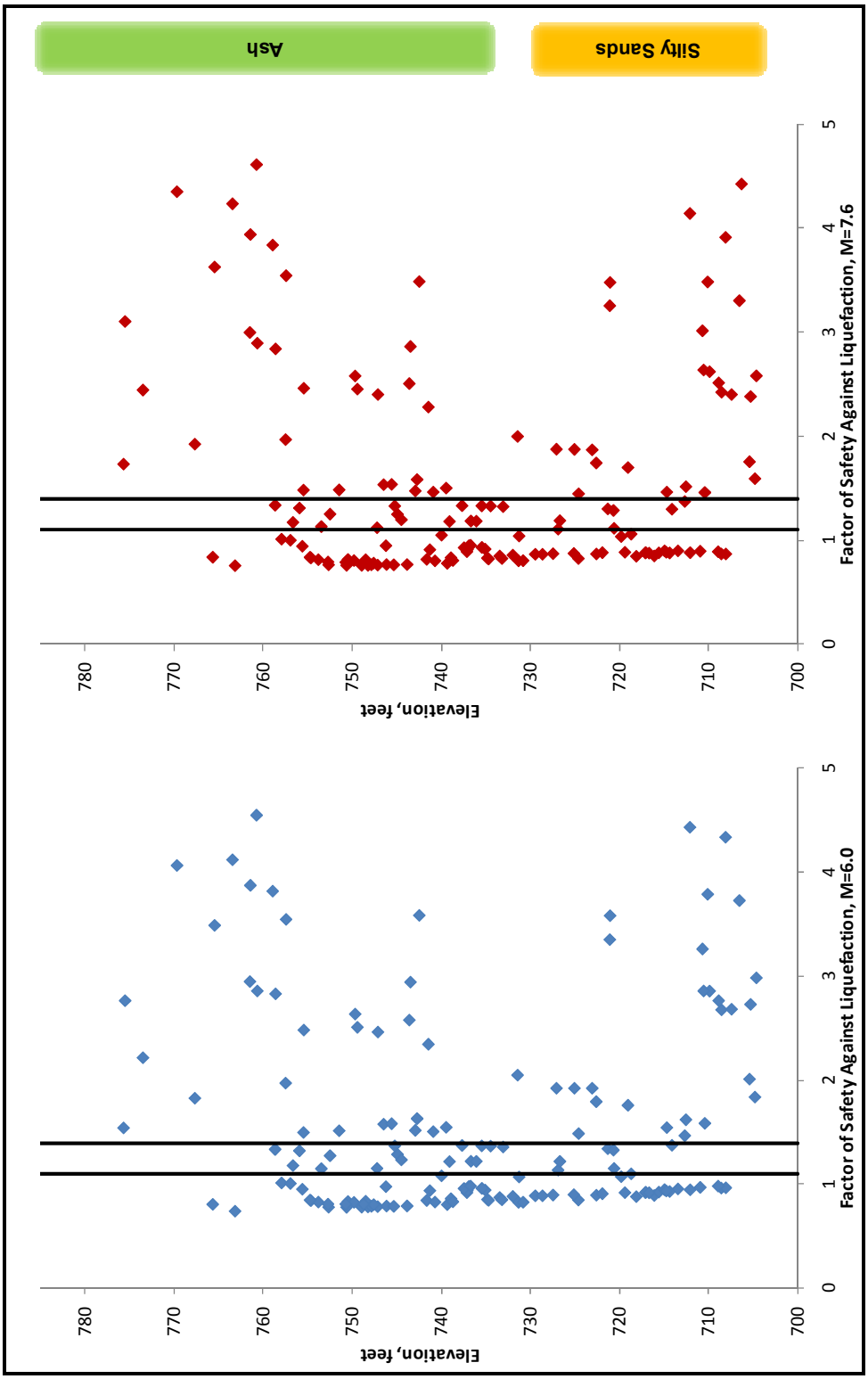

Figure 1.27 – Calculated Factors of Safety against Liquefaction (600-Series SPT Data)

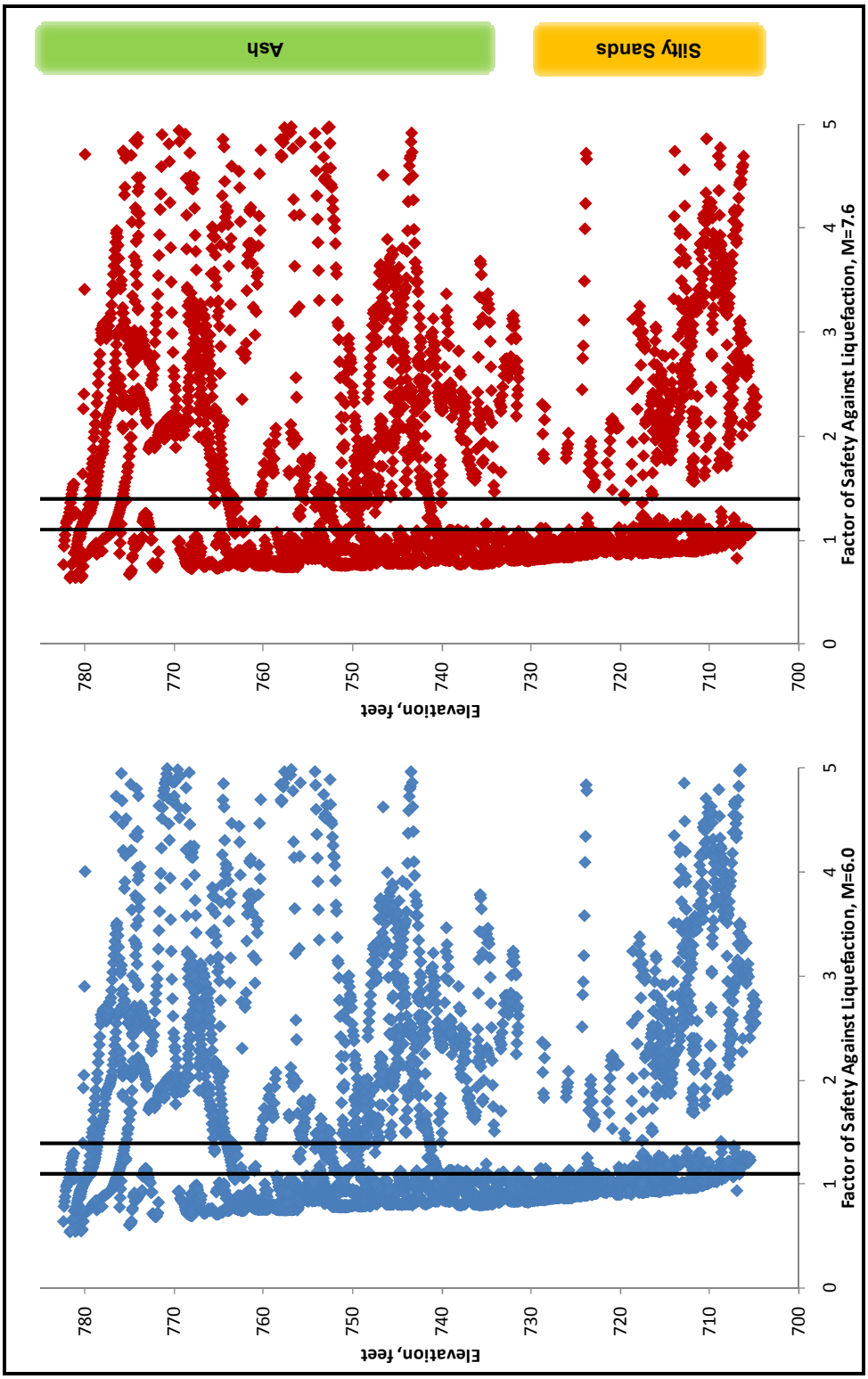

Figure 1.28 – Calculated Factors of Safety against Liquefaction (600-Series CPT Data)

Figure 1.29 – AECOM Boring Layout

References

Ambraseys, N. N. (1988), “Engineering Seismology.” *Earthquake Engineering and Structural Dynamics*, Vol. 17, pp. 1-105.

Boulanger, R. W. (2003a), “High Overburden Stress Effects in Liquefaction Analyses.” *Journal of Geotechnical and Geoenvironmental Engineering*, ASCE, Vol. 129, No. 12, December, pp. 1071-1082.

Boulanger, R. W. (2003b), “Relating K_α to Relative State Parameter Index.” *Journal of Geotechnical and Geoenvironmental Engineering*, ASCE, Vol. 129, No. 8, August, pp. 770-773.

Butler, J. J., Caliendo, J. A., and Goble, G. G. (1998), “Comparison of the SPT Energy Measurement Methods.” *Geotechnical Site Characterization, Proceeding of 1st International Conference on Site Characterization*, P. Robertson and P. Mayne (eds.), Balkema, Rotterdam, Vol. 2, pp. 901-905.

Daniel, C. R., Howie, J. A., Jackson, R. S., and Walker, B. (2005), “Review of Standard Penetration Test Short Rod Corrections.” *Journal of Geotechnical and Geoenvironmental Engineering*, ASCE, Vol. 131, No. 4, pp. 489-497.

GEO-SLOPE International, Ltd (2008). *Stress-Deformation Modeling with SIGMA/W 2007: An Engineering Methodology*. 3rd edition, March.

Hynes, M. E. and Olson, R. S. (1999), “Influence of Confining Stress on Liquefaction Resistance.” *Proceeding of International Workshop on Physics and Mechanics of Soil Liquefaction*, Balkema, Rotterdam, pp. 145-152.

Idriss, I. M. and Boulanger, R. W. (2008), *Soil Liquefaction During Earthquakes*. Publication No. MNO-12, Earthquake Engineering Research Institute, Oakland, California.

Kramer, S. L. (1996), *Geotechnical Earthquake Engineering*. Prentice Hall, Upper Saddle River, New Jersey.

Robertson, P. K. (1990), "Soil Classification Using CPT." *Canadian Geotechnical Journal*, Vol. 27, No. 1, pp. 151-158.

Robertson, P. K. and Wride, C. E. (1998), "Evaluating Cyclic Liquefaction Potential Using the Cone Penetration Test." *Canadian Geotechnical Journal.*, Vol. 35, No. 3, pp. 442-459.

Schmertmann, J. H. and Palacios, A. (1979), “Energy Dynamics of SPT.” *Journal of Geotechnical Engineering Division*, ASCE, Vol. 105, pp. 909-926.

Seed, H. B. (1983), “Earthquake-Resistant Design of Earth Dams.” *Proceeding, Symposium on Seismic Design of Earth Dams and Caverns,* ASCE, New York, pp. 41-64.

Seed, H. B., Cetin, K. O., Moss, R. E. S., Kammerer, A. M., Wu. J., Pestana, J. M., Riemer, M. F., Sancio, R. B., Bray, J. D., Kayen, R. E., and Faris, A. (2003), "Recent Advances in Soil Liquefaction Engineering: A Unified and Consistent Framework." *Proceeding of 26th Annual ASCE Los Angels Geotechnical Spring Seminar*, Long Beach, California, April 30.

Seed, R. B. and Harder, L. F., Jr. (1990), "SPT-Based Analysis of Cyclic Pore Pressure Generation and Undrained Residual Strength." *Proceeding of H. B. Seed Memorial Symposium*, BiTech Pub., Vol. 2, pp. 351-376.

Seed, H. B. and Idriss, I. M. (1971), "Simplified Procedure for Evaluating Soil Liquefaction Potential." *Journal of Geotechnical Engineering Division*, ASCE, Vol. 97, No. 0, pp. 1249-1273.

Seed, H. B. and Idriss, I. M. (1982), "Ground Motions and Soil Liquefaction during Earthquakes." *Monograph*, Earthquake Engineering Research Institute, Oakland, California.

Skempton, A. W. (1986), "Standard Penetration Test Procedures and the Effects in Sands of Overburden Pressure, Relative Density, Particle Size, Ageing and Overconsolidation." Géotechnique, Vol. 36, No. 3, pp. 425-447.

Vucetic, M. and Dobry, R. (1991), "Effect of Soil Plasticity on Cyclic Response." *Journal of Geotechnical Engineering*, ASCE, Vol. 117, No. 1, pp. 89-107.

Youd, T. L., Idriss, I. M., Andrus, R. D., Arango, I., Castro, G., Christian, J. T., Dobry, R., Finn, W. D. L., Harder, L. F., Jr., Hynes, M. E., Ishihara, K., Koester, J. P., Liao, S. S. C., Marcuson, W. F., III, Martin, G. R., Mitchell, J. K., Moriwaki, Y., Power, M. S., Robertson, P. K., Seed, R. B., and Stokoe, K. H., II. (2001), "Liquefaction Resistance of Soils: Summary Report from the 1996 NCEER and 1998 NCEER/NSF Workshops on Evaluation of Liquefaction Resistance of Soils." *Journal of Geotechnical and Geoenvironmental Engineering*, ASCE, Vol. 127, No. 10, pp. 817-833.